SYNTHESIS AND CHARACTERIZATION OF $(AlMg)B_2$- ALUMINUM BASED COMPOSITES AND NANOCOMPOSITES

by

LUVINA REYES RUSSI

A thesis submitted in partial fulfillment of the requirements for the degree of

MASTER OF SCIENCE
In

MECHANICAL ENGINEERING

UNIVERSITY OF PUERTO RICO
MAYAGÜEZ CAMPUS
2007

Approved by:

Paul Sundaram, PhD Member, Graduate Committee	Date
Nestor Perez, PhD Member, Graduate Committee	Date
O.Marcelo Suarez, PhD President, Graduate Committee	Date
Jeannette Santos, PhD Representative of Graduate Studies	Date
Paul Sundaram, PhD Chairperson of the Department	Date

ABSTRACT

The present study involves a novel method to synthesize under vacuum $(AlMg)B_2$ – aluminum based composites. Incorporation of MgB_2 into aluminum is a complex process because of the lack of wettability between both components. Aluminum high surface tension and oxide layer (Al_2O_3) formation most likely prevent magnesium diboride from mixing with liquid aluminum. High energy ball milling was selected as a key process to achieve appropriate mixing and wettability between alloy components. Many runs were completed to study processing variables such as rpm and milling time variables among others prior to get the appropriate parameters that lead to the desired mechanical mixing. Two target compositions of Al pellets (840-2400μm) and MgB_2 powder (5wt%-10wt% / 44μm) were selected at the beginning of the experimentations.

A hydraulic press was used to consolidate and compact the composite after mechanical alloying for further melting reaction (in conventional furnace) of the samples placed into evacuated quartz tubes and sealed. A good incorporation of aluminum matrix with MgB_2 produced discontinuous intermetalics particles and nanoparticles of $(AlMg)B_2$ into the aluminum matrix where eutectic Al_3Mg_2 is also present. Microstructural characterization of composite samples revealed a 2% increase in the reinforcement volume fraction Al-10wt%MgB_2 compared with the other composition at 5wt%MgB_2. Bigger particle sizes are present in the samples containing Al-5wt%MgB_2 but this composition also

presented the highest content of nanometer sized particle reinforcement leading to the highest values of Vickers microhardness. Furthermore SEM-EDS analysis helped to confirm that the ballmilling process promoted nanosized particles of $(AlMg)B_2$ composite. XRD test showed peaks associated to $(AlMg)B_2$ along with Al, AlB_2, and MgB_2 between 20° y 45°. Also this spectrum reveals the formation of Al_3Mg_2 phase, and corroborated in the micrographs. DTA curves obtained showed a dome at 820°C in the exothermic reaction associated with the dissolution of the ternary phase $(AlMg)B_2$.

Using CARIne® v3.1 software, a crystallographic modeling of $(AlMg)B_2$ phase is presented at the end of the research. As an attempt to quantify the presence of this ternary phase in the composite alloys, the XRD diffractograms of the samples were used as the starting point for the modeling analysis were a resulting stoichiometric composition of the final model is approximately $(Al_{0.5}Mg_{0.5})B_2$.

RESUMEN

La presente investigación involucra un nuevo método para sintetizar en atmósfera al vacío el compuesto con base aluminio $(AlMg)B_2$. La incorporación de MgB_2 en el aluminio es un proceso complejo debido a carencia de afinidad entre los componentes. El aluminio tiene una alta tensión superficial, sumado a la capa de alumina (Al_2O_3) que se forma externamente, evita que el diboruro de magnesio entre en contacto con el aluminio líquido. La técnica de molienda de alto impacto fue implementada como un proceso clave para conseguir que los dos materiales lograran mezclarse mecánicamente. Se completaron muchas pruebas para estudiar las variables de proceso tales como rpm y el tiempo de molienda entre otros antes de encontrar los parámetros adecuados que conllevaran a la mezcla mecánica deseada. Se escogieron dos composiciones diferentes, Al en esferas (90-95% en peso/ 840-2400μm) y polvo de MgB_2 (44μm) para desarrollar los experimentos.

Se usó una prensa hidráulica para unir y compactar el compuesto luego de la molienda mecánica y posteriormente las muestras se fueron introduciendo en tubos de cuarzo a los cuales se les hacia vacío para luego llevarlos al proceso de fundición. La adecuada integración que hubo entre el aluminio con el diboruro de magnesio produjo partículas y nanoparticulas intermetálicas discontinuas de $(AlMg)B_2$ embebidas en la matríz de aluminio en donde la fase

eutéctica Al_3Mg_2 esta también presente. La caracterización microestructural del compuesto desarrollado reveló un aumento de 2% en el valor de fracción de volumen de refuerzos comparado con la otra composición de 5wt%MgB_2. Por otra parte la aleación Al-5wt%MgB_2 mostró las partículas más grandes de refuerzo pero esta composición también mostró los contenidos mas altos de nanopartículas de refuerzo promoviendo con esto valores más altos de microdureza Vickers. Adicionalmente los análisis efectuados en el microscopio SEM/EDS ayudaron a confirmar que la molienda de alto impacto promovió la formación de nanoparticulas de $(AlMg)B_2$. Los análisis de difracción de rayos X de la aleación mostraron picos asociados al sistema ternario dado que se presentaron cercanos a los picos de Al, AlB_2, MgB_2 entre 20^o y 45^o. Asimismo estos espectros revelaron la fase eutéctica Al_3Mg_2 corroborada en las micrografías. Los análisis de diferencial térmico DTA obtenidos mostraron un domo a 820ºC en la reacción exotérmica asociado a la disolución del sistema ternario $(AlMg)B_2$.

Usando el programa CARIne® v3.1, se desarrollo un modelamiento cristalográfico de la fase $(AlMg)B_2$ el cual se presenta al final de la investigación. En un esfuerzo por modelar cuantitativamente la presencia del sistema ternario en el compuesto, los difractogramas de las muestras procesadas fueron usados como punto de partida para este modelamiento donde se obtuvo una composición estequiometrica aproximada de $(Al_{0.5}Mg_{0.5})B_2$.

To the infinite light of love
And engines of my life:

Lyannie Susane
And
Lorein Fernanda

ACKNOWLEDGEMENTS

I wish to thank my advisor Dr. Oscar Marcelo Suarez for provide a conductive environment in this very interesting research area of the Aluminum matrix composites and whom I have learned incalculably and benefited greatly in understanding to complete this research. I'm also grateful because of his friendship and so for his *patience* throughout this endeavor.

Thanks to the Department of Mechanical Engineering, Dr. Paul Sundaram, to all my professors throughout my graduate studies, PREM (partnership for research and education in materials) and the University of Puerto Rico at Mayaguez from all that I learnt.

Also I'm so grateful with Michael Ramirez and Gabriel Cruz from the SEM-Laboratory of Hewlett Packard, Aguadilla, who helped me in the use of those facilities to analyze my samples.

In this journey I had the good fortune to interact with a many colleagues, I would like to thank all of them for their help I'm deeply grateful, especially under graduate student José Vázquez from the mechanical engineering department and graduate student Richard Pérez Moyet from physics department.

Thanks to my parents, brother and sisters for their help, love and voices of strength.

To Michael and Jeannette to be a family for my daughters and me during this time in Puerto Rico.

And last but not least, thanks a lot to Sandra Pedraza T, to be my friend and sister in the most difficult moments.

This research is based upon work supported by the National Science Foundation under Grant No. 0351449.

Table of Contents

List of Figures

List of Tables

Tables **Page**

ACRONYMS USED IN THE RESEARCH

Some terms have been coined to explain process in the present research. The following list explains the expansions of some of the most commonly used acronyms:

AMC	aluminum matrix composites
BM	ball milling
BPR	ball-to-powder weight ratio
DTA	differential thermal analysis
EDS	Energy dispersed X-ray spectroscopy
FCC	face centered cubic
HEBM	high energy ball milling
HV	microhardness Vickers
MA	mechanical alloying
MM	mechanical milling
MMC	metal matrix composites
PCA	process control agent
PSD	particle size distribution
SEM	scanning electron microscopy
TA	thermal analysis
TGA	thermo gravimetric analysis
XRD	X ray diffraction

1 INTRODUCTION

The aerospace industry is continuously pursuing to enhance the performance of commercial and military aircraft and thus, driving the development of better high performance structural materials. In recent years, metal matrix composites (MMC) have emerged as a promising class of such materials. MMCs often have a relatively ductile metal matrix phase and a significantly harder reinforcement material like ceramics or refractory metals. The matrix holds the reinforcement material together and provides ductility while the reinforcement imparts strength and stiffness to the composite. A common problem with MMCs is the difficulty in creating a strong matrix/reinforcement interface without suffering extensive dissolution, debonding, or chemical reactions [1]. A proposed solution is the use of a reinforcement material which is similar in chemistry to the matrix. Many studies have been dedicated to aluminum and its alloys as matrix due to their lightweight cost, and their unique thermal properties that have enormous space and avionics prospects [2].

This research is aimed at creating an AMC reinforced with $(AlMg)B_2$ particles. AMC mixed with MgB_2 have importance to be studied widely because the impact of a soft and low density of the matrix reinforced with hard particles and nanoparticles of $(AlMg)B_2$ that have been exploited as reinforcements, can be proposed for aerospace applications as a good alternative where materials with light weight and wear resistance is required. The recent discovery of

superconductivity in MgB_2 at 39ºK in 2001 has increased the scientific importance of AlB_2-type borides; furthermore aluminum diboride is one of many stable crystalline phases naturally present in the Al-B system [3].

1.1 Literature Review

Precipitation hardening in Al alloys has been known for several decades and applied to numerous systems [4]. Aluminum diborides and magnesium diborides have been studied by many researches [5]. Like most transition metal borides, they crystallize in the simple AlB_2-type structure hp3 which is usually described as a stacking of intercalated graphite-like boron sheets and hexagonal layers of the metal atoms. Despite the great interest in the understanding of the origin of all these characteristics, and the potential use of borides for high-performance applications, many of their physical properties have not been studied extensively: such as mechanical properties, mainly hardness, and wear resistance that deserve more intensive investigation.

Hofmann [5](1969) mixed borides of lithium, magnesium and aluminum in order to study the formation of $(Al,Mg)B_2$ solid solution. After sintering in argon at temperatures between 725ºC and 790ºC the formation of such a solid solution was identified despite the kinetic difficulty of formation [5].

Matkovich and Economy [6] (1980) prepared $MgAlB_{14}$ by heating a mixture of magnesium, aluminum and boron in atomic proportions of 1:2:14 to 900ºC for 6 h. The sample was then cooled and treated with concentrated hydrochloric acid. The crystal structure of this phase was determined by X-ray diffraction.

Vekshina et al (1981) mixed 99.9% pure metals of aluminum and magnesium with 99.2% pure amorphous boron to obtain 22 compositions. The mixtures were briquetted and heated to temperatures of 850 to 1000ºC under an argon atmosphere in sintered alumina crucibles. The reaction products were investigated by X-ray phase analysis. They found that $MgAlB_{12}$ is identical to $MgAlB_{14}$ [5].

Hall (2000) reported a new family of metal matrix composites (MMC's) based on high aspect ratio AlB_2 [4]. The preparation of these MMC's involved the conversion of low aspect ratio AlB_2 to high aspect ratio AlB_2. This conversion is associated with the $Al(L) + AlB_{12} \leftrightarrow AlB_2$ peritectic transformation. The peritectic temperature was investigated using calorimetric methods and determined to be 956 ± 5 °C. In addition, an unexpected conversion of low aspect ratio AlB_2 to high aspect ratio AlB_2 was identified near the peritectic temperature [6].

Bussmann and Bianconi (2003) studied the effects of diborides in the amplification of the Tc critical temperature by quantum interference for the system $Al_{1-x}Mg_xB_2$ by tuning x from MgB_2 to $AlMgB_4$ [7].

Although there are publications concerning the alloying between Al, Mg and B, the main basis of these studies were the use of boron as a grain refining to the Al-Mg alloys. Those researches have in common the crystal studies by using XRD for characterization that helped build up the ternary phase diagram. None of the previous researches have implemented the ballmilling process to reach mixing between components, and they report different synthesis process. There are no previous reports of reinforcement particles sizes and furthermore previous studies do not report $(AlMg)B_2$ nanoparticles formation.

The present research implements a brand new method to achieve mixing between aluminum and magnesium diboride, which is the ball milling process. The achievement of $(AlMg)B_2$ ternary phase will be confirmed by EDS analysis an the particles formation down to 100nm will be also presented.

1.2 Research Objectives

Due to the difficult to obtain wettability between Al and MgB_2, the aim of the present research was to develop a process to achieve enough mixing for further synthesis between Al (pellets) and MgB_2 (powder) to achieve AlB_2 and/or $(AlMg)B_2$ composites with an Al matrix under vacuum. Two different compositions Al-5wt%MgB_2, 10wt%MgB_2 were selected to be synthesized and characterized. The synthesized material was examined in terms of microstructure, physical and mechanical properties. Particular emphasis was placed to correlate the improvement in physical and mechanical properties of elemental aluminum with the presence of the reinforcement.

Specific objectives are the following:

- Standardize the ball milling parameters that leads to an appropriate mixing and mechanical alloying between the components Al pellets and MgB_2 powder
- Design and assemble a process to obtain the samples under vacuum for the melting process.
- Obtain $(AlMg)B_2$ particles and nanoparticles reinforcements in the Al matrix after the heating cycle

- Characterize the microstructure of the new composite, its volume fraction, particle size and microhardness Vickers.
- Extend the analysis to XRD, DTA and SEM/EDS techniques to corroborate crystallographic phases present, thermal phase changes and nanoparticles size and chemical composition, respectively.

1.3 Outline of the research

Chapter 2 deals with the theory of ball milling process, and a summary on the aluminum matrix composites and the binary systems involved in the present research as well as the ternary system Al-Mg-B. Chapter 3 presents the complete procedure, as designed and developed to achieve the synthesis of the $(AlMg)B_2$ and Al composite at each process steps, i.e. ball milling, samples compaction, sealing and evacuating quartz tubes and finally melting reaction. Chapter 4 presents the characterization process and the data analysis. Conclusions are showed in the fifth Chapter, and finally the Chapter 6 presents various recommendations for further research with the same starting elements (Al and MgB_2) and improving the process.

2 THEORETICAL BACKGROUND

2.1 Mechanical alloying by ball milling

2.1.1 General description

Mechanical alloying, MA, was developed in 1960 by the International Nickel Company (INCO) as a technique for dispersing nanosized oxide inclusions into nickel- based superalloys for gas turbine applications. The ball milling process has been successfully used and accepted as an industrial processing method because it is a simple, scaleable and inexpensive technique to prepare a variety of equilibrium and non-equilibrium alloy phases, including solid solutions, intermetalics, quasycristals, nanostructured materials, amorphous alloys and bulk metallic glasses of commercially useful and scientifically interesting materials with a number of novel properties [8].

Mechanical alloying is a process involving repeated cold welding, fracturing, and rewelding of powder particles in a high-energy ball mill. Such a process can result in the formation of an alloy with nanometer-sized grains.

During the mechanical alloying process, the powder particles are periodically trapped between colliding balls and are plastically deformed. Such a feature occurs by the generation of a large number of dislocations as well as other lattice defects. Furthermore, the ball collisions cause fracturing and cold

welding of the elementary particles, forming clean interfaces at the atomic scale. This leads to an increase of the interface number while the sizes of the components area decrease from millimeter to sub micrometer dimensions. Concurrently to this decrease of the elementary distribution, some crystalline and nanocrystalline intermediate phases are produced inside the particles involving chemical changes [9]. For the present research the parent materials are aluminum pellets and magnesium diboride powder which cannot be mixed by regular melting and casting.

The most important attributes of mechanical alloying are the following:

- Production of fine dispersions of second-phase particles
- Extension of solid solubility limits
- Refinement of grain sizes down to nanometer range
- Synthesis of novel crystalline and quasi-crystalline phase
- Development of amorphous (glassy) phase
- Disordering or ordered intermetallics
- Fabrication of materials with a precise composition and controlled microstructure
- Possibility of alloying elements difficult to combine by conventional melting methods
- Inducement of chemical reactions at low temperatures
- Scalable process

2.1.2 Process variables in milling

To achieve the adequate product phase, microstructure, particle size and/or properties, the optimization of a number of variables involved during MA has to be considered. The following variables have an important effect in the final product after ball milling:

- Milling container (vial, jar, vessel, bowl)

Hardened steel, tempered steel, stainless steel, tungsten carbide, are the most common types of materials used for the grinding vessels. The material of the jar can alter the composition of the material to be mechanically milled because of the high impact and wear. The internal design of the container is important to avoid dead zones, or where the composition does not get milled; flat ended or round ended jars are used.

- Milling atmosphere

To avoid contamination and to minimize oxidation of the milled powder, MA can be conducted under vacuum or under an inert atmosphere (nitrogen/argon). The atmosphere influences the kinetics of alloying behavior of transformations and new compounds formation.

- Milling speed

Milling intensity or milling energy are terms used to describe the velocity of the milling process. The faster rotation of the milling the higher input energy into the material being processed i.e. higher kinetic energy of the grinding medium imparted to the composition upon ballmilling [8]

$$E = \frac{1}{2} m v^2 \qquad \textbf{(2.1)}$$

Where m, is the mass and v, is the relative velocity, both of the grinding medium). Increasing the milling speed results in excessive wear of the milling tools and leads to the contamination of the material composition. Additionally, the temperature of the jar may reach a high value accelerating the transformation process by forming supersaturated solid solutions or metastable phases. When a critical speed occurs, the balls are pinned to the inner walls of the jar and do not fall down to exert any impact force, so the maximal speed should be below that critical value to ensure the maximal collision energy. High speed can promote higher degree of plastic deformation and cold welding so the material gets stuck to the inner walls of the container.

The milling intensity or speed can be described as a function of ball to powder weight ratio (BPR) **(=** M_b / M_p **)**, the velocity and frequency of the balls as follows: [8]

$$I = M_b V_{\max} f / M_p \quad \textbf{(2.2)}$$

Where M_b is the mass of the balls; M_p, the mass of the material to be milled in the jar; $V_{\max}$ the maximum velocity of the balls and f, the balls impact frequency.

- Grinding medium

This parameter affects directly the efficiency of the alloying. The impact force on the powder should be high enough to promote mixing and mechanical alloying, and is affected by the size, density and material of the balls. High density of the grinding medium represents high kinetic energy to be transferred to the powder. Materials commonly used are hardened steel, hardened chromium steel, stainless steel, and WC-Co. (figure 2.1). Small ball sizes (soft milling) promote intense frictional action which benefits the formation of solid solutions and amorphous phases in the final constitution. Also the attained grain size is finer with smaller balls. Large ball sizes (hard milling) result in only the mixing of components and produce high temperature which leads to the decomposition of metastable solid solutions.

To “randomize” the motion of the balls and produce shearing forces a combination of small and large balls can be used. This technique helps to reduce formation of cold welding in to the jar walls and balls surface.

Figure 2.1 Vial- balls- lid-gasket set [9]

- Extent of container filling

To permit the movement and energy of impact forces exerted on balls and powder particles, enough free space in the jar is essential. About 50% of the vial space is left empty.

- Ball-to-powder weight ratio (BPR)

Sometimes BPR is referred as the charge ratio, an important variable that affects the time of process. It varies from a value as low as 1:1 to one as high as 100:1. Those ratios depend on special desired features, crystalline sizes, particular phase formation, microhardness and other final results. The higher the BPR the shorter milling time and faster MA. At a high BPR the mean free path decreases, and the plastic deformation increases by the increment in number of collisions per unit time; so more energy and temperature is transferred to the powder particle resulting in a faster alloying. Higher BPR can be obtained also

without changing the number of balls but increasing the diameter of them or by using higher density of materials such as WC rather than steel. Lower ball to powder weight ratio results in longer times of processing to reach specific properties but increases the amount of material processed and its crystalline size.

- Milling time

This is one of the most important parameters and is chosen to achieve a steady state between fracturing and cold welding of the materials in the container to facilitate the alloying. Times of process are short for high BPR values and extended for low BPR values, as explained previously.

2.1.3 Equipment for ballmilling

There are different machines available for mechanical alloying. These differ in their capacity, speed of operation, efficiency of milling and additional arrangement for cooling, and heating among others.

- The Spex shaker mill is used for exploratory investigations in the laboratory and screening purposes. It has one jar containing the grinding and powder sample. The jar moves describing a shape of an infinity symbol (∞) energetically several thousand times per minute.

- The planetary ball mill was employed in the present research (figure 2.2).

This type of ball milling equipment is used to produce less than hundred grams of powder. Its name represents the planet-like movement of its two jars on a rotating support disk. Both jars rotate around their own axes.

Figure 2.2 Fritsch Pulverisette P4™ Vario-planetary ballmilling machine with two vials mounted on supporting disk [9]

The containers and the supporting disk rotate in opposite direction producing centrifugal forces that alternately act in the same and opposite directions (figure 2.3). This causes two different effects:

- Friction effect: The grinding balls run down inside jar walls
- Impact effect: The sample material and balls lift off and travel freely through the inner container and collide with the opposite walls. This effect

increases each time the balls crash one onto another. The impact energy depends on the speed (RPM) selected and can reach 20 times the acceleration of gravity. If the speed is reduced the impact energy is reduced and only mixing occurs.

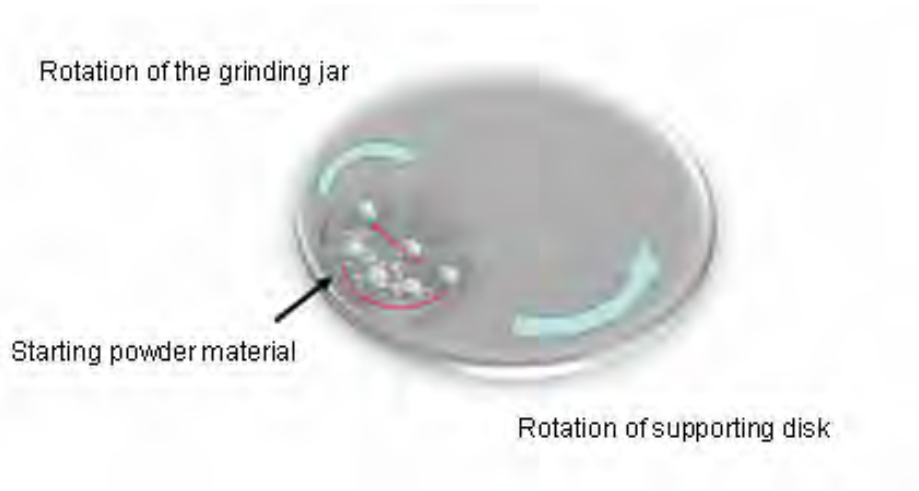

Figure 2.3 Representative motions inside the jar of planetary ball milling

- The attritor mill is used for large quantities of powders milled at a time and consists of a vertical drum containing a series of rotating impellers moved by a powerful engine. The impellers agitate the steel balls into the drum at a high velocity to impact the powder.

2.1.4 Mechanism of alloying

Different types of materials including ceramic, metallic, polymer and composites are synthesized by ball milling. A large number of phases can be

formed depending on each alloy system. The mechanism through which the new alloy phases are reached is explained below.

During the collisions ball-powder-ball the powder for MA is subject to heavy deformation into the grinding medium. The powder particles are repeatedly flattened, cold welded, fractured and rewelded. For ductile materials, the effect of the collision produce material gets flattened whereas the brittle intermetallic gets fragmented and size refined (figure 2.4).

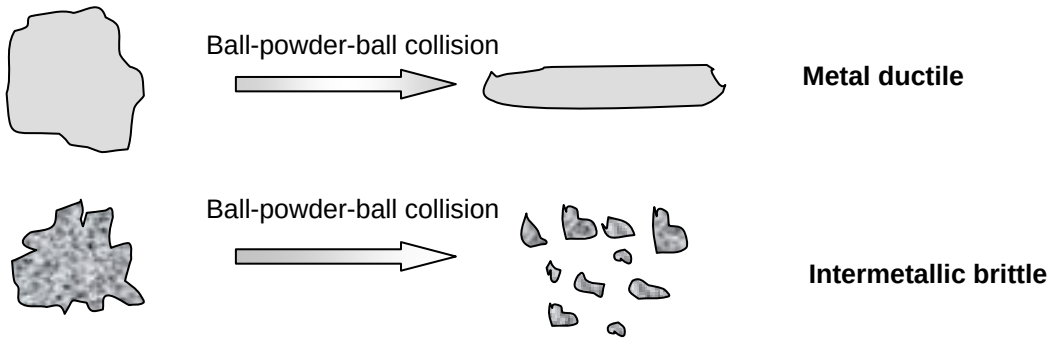

Figure 2.4 Deformation characteristics of different starting materials for BM

Every time two grinding balls smash or collide together, a small amount of powder or material is trapped between them and goes through three different stages. On average, around 1000 particles are trapped during each collision.

Throughout the process of BM the powder morphology is modified in two dissimilar ways. If the starting material is ductile form layers that overlap

structuring composite cold welds between them with different composition. The brittle constituents have a tendency to become occluded by the ductile component and trapped in the composite. These processes of cold welding and fracturing occur continually during the milling time leading at the end to a homogenized and refined composition. (Figure 2.5)

In the early stage of the process, the chemical composition of particles varies significantly from particle to particle. The prevalence in the first stage is a lamellar structure with particle sizes that varies from few micrometers to few hundred micrometers.

In the intermediate stage as the milling process continues more cold working takes place accompanied with microstructural refinement, introduction of vacancies, dislocations, and grain boundaries. Diffusion paths are created by an increase in temperature due to the collisions between powder and ball-ball / ball-wall. Alloy formation occurs in this stage.

During the final stage the lamellae microstructure becomes uniform, finer with a homogeneous composition achieving a steady state. The microhardness of the particles attains a high level due to the strain energy accumulated during the process.

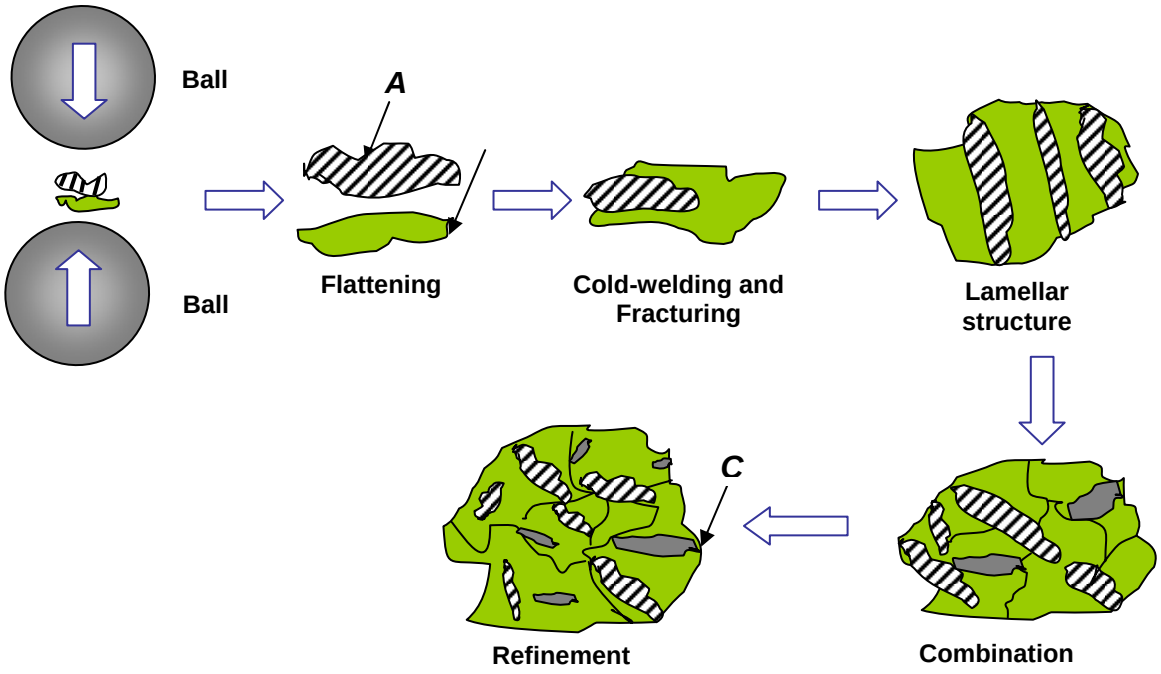

Figure 2.5 General behavior of powder particles *A, B* and formation of a new phase *C*

2.1.5 Systems of alloy components

Different types of materials used for mechanical alloying lead to the following classification, which depends on the mechanical properties of the components:

- Ductile-ductile components

As literature mentions, is necessary to have at least 15% of ductile component to achieve alloying. A true alloying results from the repeated action of cold welding that only occurs if the particles are ductile. In the first stage of

processing this system, a small amount of material gets welded onto ball surfaces, preventing excessive wear of the grinding medium. The flattened particles form lamellar structure from random welding. At the end of the process a homogeneous structure is formed and the powder can be removed from the grinding medium.

- Ductile-brittle components

At the first stage of milling the ductile material get flattened by the balls collisions while the brittle particles get fragmented. These fragmented particles tend to become fitted and trapped by the ductile particles as explained above. This system fits to the present research, where the ductile component is aluminum pellets and the brittle component is magnesium diboride powder.

- Brittle-brittle components

In this system the particles get fragmented and their particle size reduced constantly. The harder component gets embedded in the softer component, but alloying is not possible in this case.

2.2 Aluminum matrix composites (AMC) and review of relevant boride phases in the (AlMg)B_2 system

AMCs belong to the metal matrix composite (MMC) family that will be described in the following paragraphs.

2.2.1 Description of metal matrix composites (MMC)

Metal matrix composites cover a relatively wide range of materials defined by the metal matrix, reinforcement geometry and type. In the matrix field, most metallic systems have been studied and explored. They include aluminum, beryllium, magnesium, titanium, iron, nickel, cobalt, and silver but aluminum is by far the preferred one [10].

MMCs consist of at least two constituent parts, the major percentage of one being a metal and the other part may be a different metal or another material, such as a ceramic or organic compound. When at least three materials are present, it is called hybrid composite. An MMC is complementary to a cermet. These engineering materials can attain higher strength, greater stiffness, and better dimensional stability than the unreinforced metal alloys which promoted the development of varied kinds of MMC of low cost, lighter and stronger than their original alloys [2]. Incorporating the two materials (the matrix and the reinforcement materials) result in remarkable structural and physical properties. In a metal matrix composite the two constitutive parts are:

- The matrix, which is the monolithic material where the reinforcement is embedded, and is fully continuous. Furthermore there is a pathway through the matrix to any point in the material where dissimilar two materials sandwiched together. The matrix is usually a lighter metal such as aluminum, magnesium, or titanium, and provides a compliant support for the reinforcement to be used in structural applications.

- The reinforcement is embedded into the matrix and can be divided into five major categories: continuous fibers, discontinuous fibers, whiskers, particulates, and wires. Reinforcements generally are ceramics with the exception of wires, which are metals. They can be either continuous, or discontinuous.

1. Discontinuous MMCs can be isotropic and worked with standard metalworking techniques. These use whiskers, short fibers, or particles. The most common reinforcing materials in this category are alumina and silicon carbide.

2. Continuous reinforcement uses monofilament wires or fibers such as carbon fiber or silicon carbide. Because the fibers are embedded into the matrix in a certain direction, the result is an anisotropic structure in which the alignment

of the material affects its strength. Some of the first MMCs used boron fibers as reinforcement.

The wide diversity of MMCs has properties that differ dramatically. The factors influencing their characteristics include: matrix and reinforcement properties, form, geometric arrangement, volume fraction, including effects of porosity and the interface between the matrix and reinforcement.

2.2.2 Description of aluminum matrix composites (AMC)

AMCs are the most important and attractive non-ferrous matrix materials used particularly in the aerospace and transport industry where light weight of structural components is crucial. Aluminum composites have unique thermal and conductive properties with coefficient of expansion that can be tailored down to zero. Parameters like the matrix alloy and reinforcement material, and volume, shape and location of the reinforcement, as well as the fabrication method can all be varied to achieve required properties [2]. Regardless of the variations, however, aluminum composites offer the advantage of low cost over most other MMCs. In addition, they offer high shear strength, excellent abrasion resistance, high-temperature operation, nonflammability, minimal attack by fuels and solvents, and the ability to be formed and treated on conventional equipment. They are very attractive for their isotropic mechanical properties (higher than their unreinforced alloys) and their low costs, cheap processing routes and low

prices of some of the discontinuous reinforcement such as SiC particles or Al_2O_3 short fibers.

2.2.3 Binary systems involving the constitutive alloying elements: Al,Mg and B

This section is divided in three parts. The first part describes the MgB_2 system. The second part is related to the Al-B phase diagram and the third refers to the Al-Mg system.

- Magnesium Diboride: Superconductivity below 39°K in MgB_2 was discovered in 2001, a high transition temperature for a relatively simple Intermetallic compound: only three atoms per hexagonal unit cell with an hp3 crystal structure [11]. Simple crystal growth of MgB_2 appears to be inflexible. Fortunately, MgB_2 can be synthesized by a simple alternate route: reaction of B with Mg vapor, generally at a temperature of about 900ºC for as little as a couple of hours. Magnesium melts at 652ºC, the reaction mechanism is considered to be moderated by magnesium vapor diffusion across boron grain boundaries. MgB_2, crystal structure forms graphite-like honeycombed layers. Magnesium atoms are located above the centre of the hexagons in-between the boron planes. (Figure 2.6). The layered crystal structure of MgB_2 produces anisotropic properties when fields and electric currents are applied in various directions with respect to the boron planes. The reason for this behavior is that the Mg ions donate electrons to the conduction band but the Mg atomic orbital play only a small role in the

conduction process; the honeycomb planes of B determine the electronic properties [11].

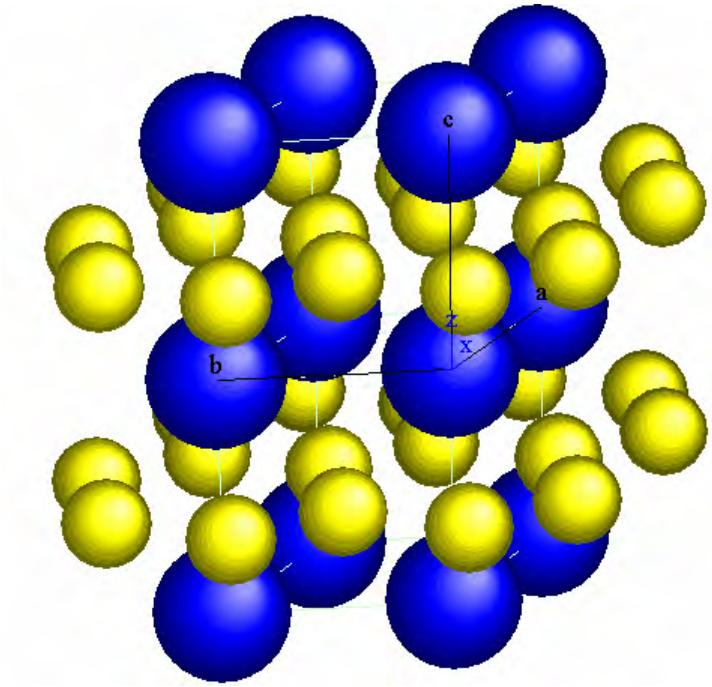

Figure 2.6 MgB_2 crystal structure modeled with CARIne software (Blue atoms: Mg, Yellow atoms: B [12]

MgB_2 density is comparable to aluminum perhaps leading to new lightweight applications. Yet, MgB_2 is hard to synthesize by conventional methods; furthermore, it decomposes rather than melts and does not have any accessible liquid-solid transitions at ambient pressures. Figure 2.7 shows an accepted phase diagram between Mg-B elements.

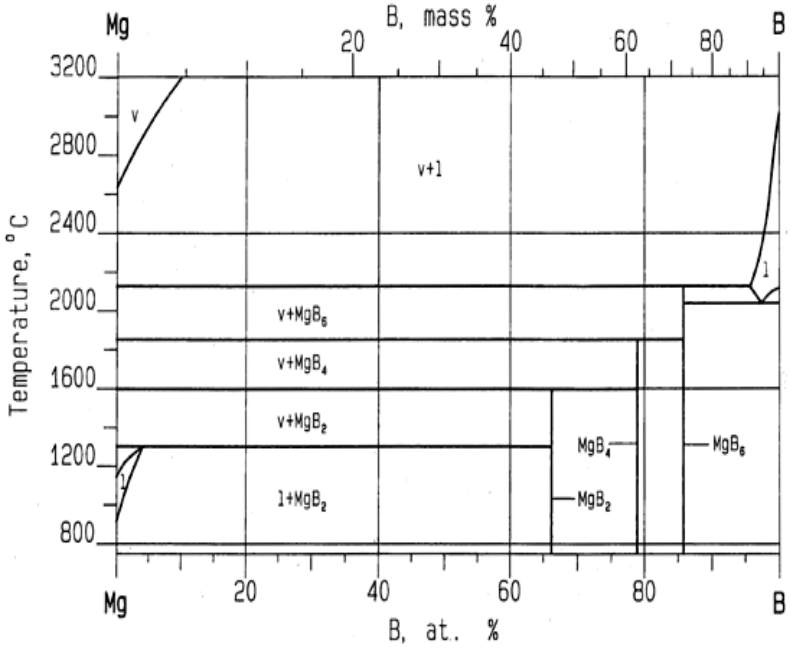

Figure 2.7 Squematic binary phase diagram for Mg-B system [5]

- Aluminum diboride: In the case of aluminum matrix composites, the AlB_2 is the prototype compound with the same hp3 structure as MgB_2 and is a stable crystalline phase naturally present in the alloy system, which has been used as reinforcement [2]. Reinforcement volume fraction can be varied from 0 to 20% by control of alloy composition and by the use of a modified squeeze casting apparatus. At 20v/o loading of AlB_2 an 80% increase in strength over the matrix alloy was observed. Wear and creep resistance of these composites is also found to be excellent. Figure 2.8 shows the Al-B equilibrium phase diagram. The liquidus line in the Al-B phase diagram evinces the practical insolubility of boron in the aluminum matrix. Experiments studying thermal behavior in all composition ranges in the binary Al-B system revealed at least seven invariant temperatures but for the present research the most important ones are the eutectic and the

peritectic transformations. The presence of the eutectic reaction is found at L↔(Al) + AlB_2 (659°C). Differential thermal analysis confirmed the peritectic formation of AlB_2 at 1030°C from Al(L)+αAlB_{12}. AlB_2 and AlB_{12} are the only true binary aluminum boride compounds [13]. As in the MgB_2, the AlB_2, (figure 2.9) has the aluminum atoms located at the center of hexagonal prisms that are formed by boron layers [7].

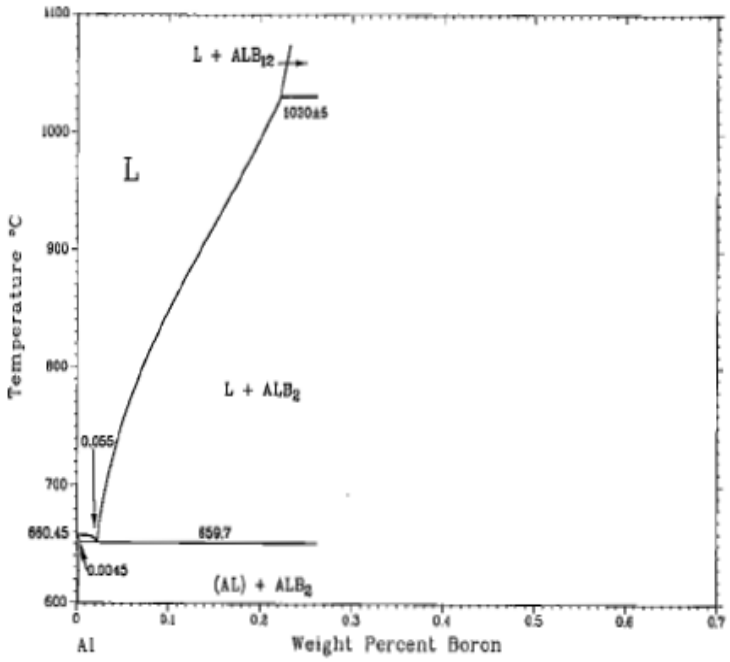

Figure 2.8 Al-B squematic binary phase diagram [13]

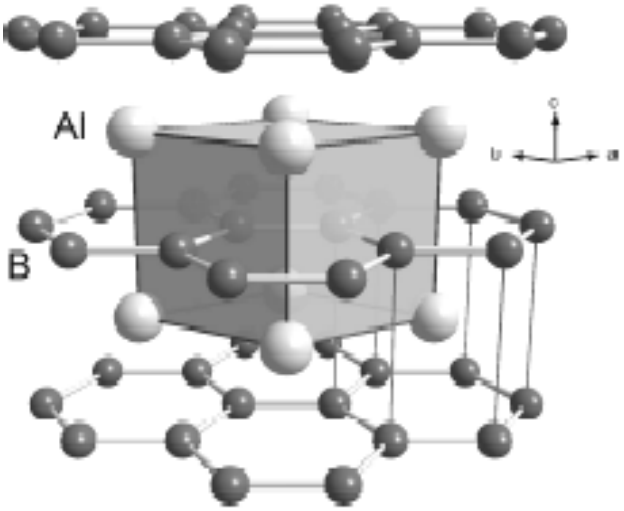

Figure 2.9 Crystal structure of aluminum diboride [14]

- Al-Mg binary system: This alloy system is usually produced for scientific purposes rather than for large-scale consumption [15]. Mg is added to aluminum to increase strength. Aluminum-magnesium alloys with Mg concentration on the order of or below 5% are solid solutions, with the substitutional Mg solute randomly distributed in the matrix. Although at room temperature a thermodynamic driving force for the formation of the intermetallic phase Al_3Mg_2 exists, the kinetics of its formation is very slow.

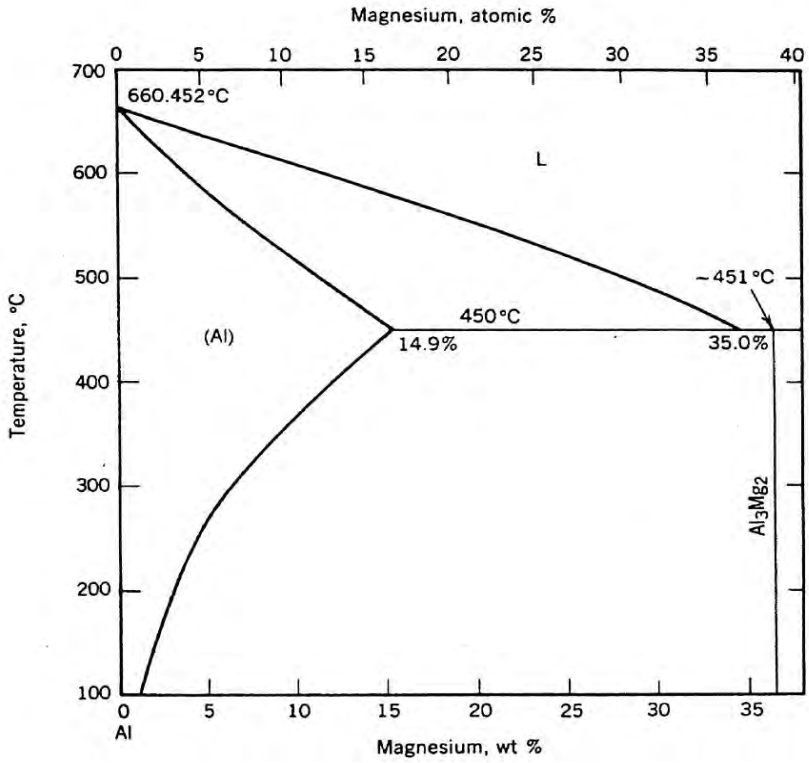

Figure 2.10 Al-Mg phase diagram [16]

Over 7%Mg at room-temperature precipitation occurs leading to the increment in strengthening by work hardening in the alloy. The aging treatment has no influence on the mechanical properties. The precipitate in equilibrium $Al_3Mg_2(\beta)$, is observed at 451°C, and at 37.3wt%Mg. (figure 2.10).

Mg decreases the density of Al linearly by approximately 0.5% for every 1%wt% Mg in solid solution [17]. Mg has a high solid solubility in solid aluminum at 450° C up to 14.9 wt%; this solubility decreases to approximately 1.7 wt% at room temperature. Yield strength and ultimate tensile strength increase with

increasing Mg content at the same time as elongation drops sharply with even small Mg additions.

2.2.4 Al-Mg-B ternary system

One of the few reported ternary phase diagrams of Al-Mg-B is shown in figure 2.11 at an isothermal section of approximately 900ºC [5]. A complete phase diagram does not exist in spite of several groups investigated the interaction in the ternary system.

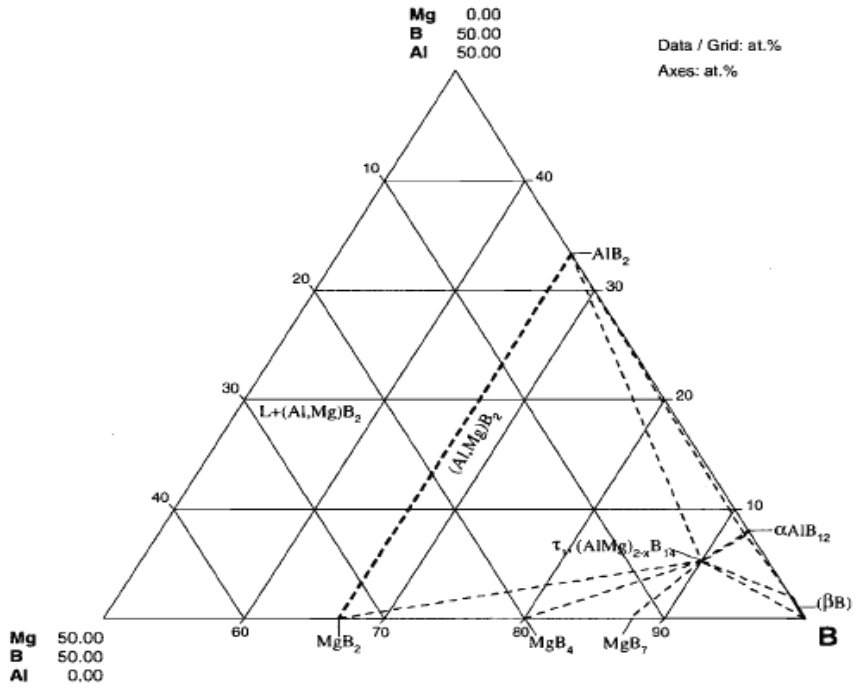

Figure 2.11 Ternary phase diagram for Al-Mg-B at isothermal 900ºC [5]

Figure 2.11 is representing compositions up to 50% of each component (Al,Mg,B). The figure 2.12 is an extension up to 100% of the ternary phase diagram to locate the composition selected in this research. The red and green points represent the expected composition to Al-10wt%MgB_2 and Al-5wt%MgB_2 mixture. Some properties of the three elements and their binary alloys of the present research are showed in the table 2.2.

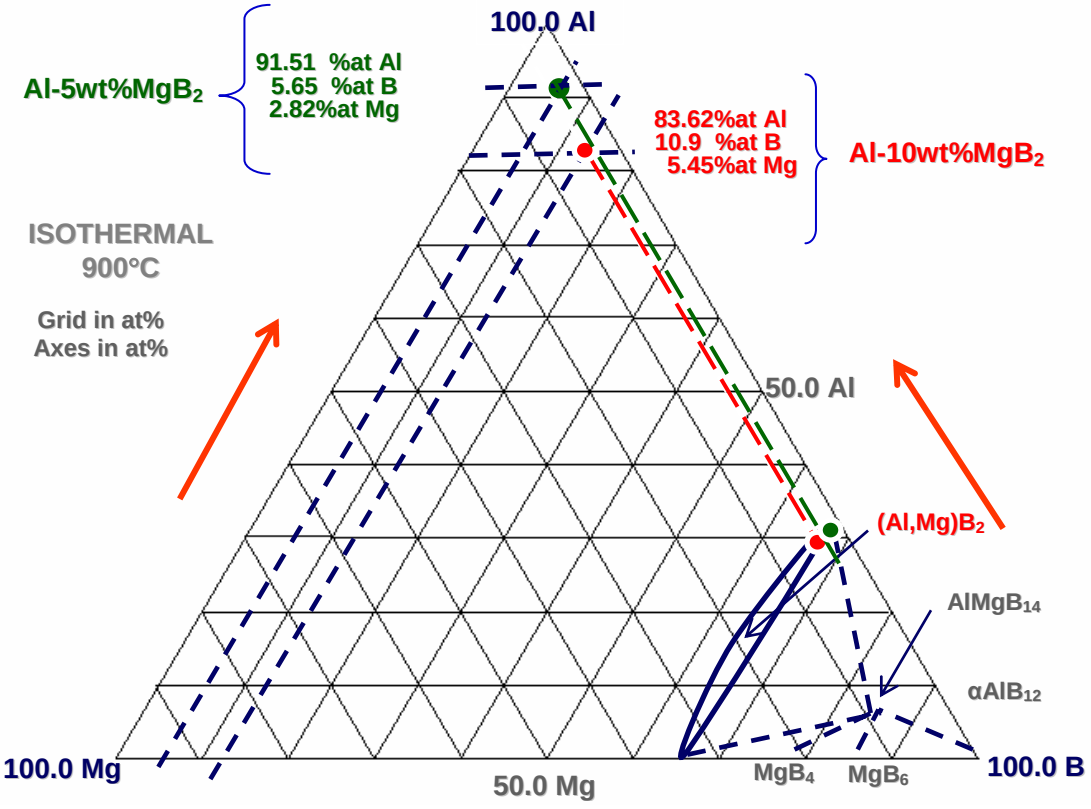

Figure 2.12 Extended ternary phase diagram for Al-Mg-B

Table 2.1 Properties related to the binary systems [2],[10],[17]

Element	Density	Melting Point	Crystalline System	Hardness
	g/cm^3	^{O}C	Bravais Lattice	Gpa
Al	2.11	660	FCC	2.3
Mg	1.74	660	HCP	2
B	2.31	2100	RHOMBOEDRAL	9.5
AlB_2	3.19	1655	HCP	
MgB_2	2.62	1300	HCP	
Al_3Mg_2	2.37	600.45	CUBIC	

2.3 MMC interface bonding and wettability

The interface in a MMC is the area linking the matrix and reinforcements. The boundary separating these two phases is where there exists dissimilarity in chemical or physical properties [1],[20]. The type of interaction at the interface will greatly influence the mechanical properties of the composite. It is important to understand the term wettability and the modes of interface bonding in MMCs in order to create a material with superior mechanical properties.

Wettability is the term which defines the degree to which a liquid drop will spread on a solid surface, and can be measured by the sessile drop test. The wettability concept is important in understanding bonding theory between the matrix and reinforcement in MMCs. Wettability refers to the extent of intimate contact possible at the molecular level [19]. Figure 2.13 shows a representation

of this concept. An appropriate interface bonding is implied when there are uniform atomic or molecular bonds along the boundary.

Wetting is not usually measured for the MMCs, but the concept is a vital tool to improve the quality of interface bonding [19].

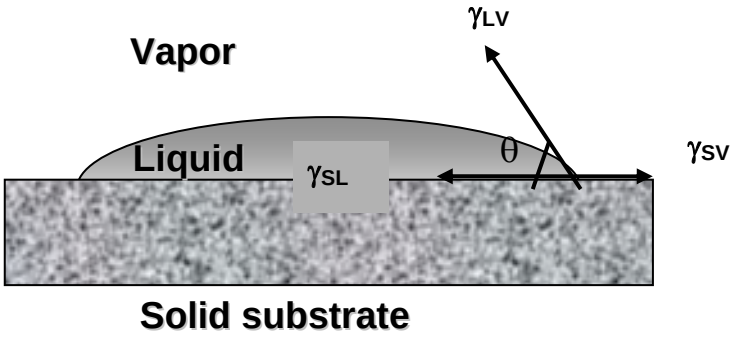

Figure 2.13 Contact angle θ and the surface energies γ for a liquid drop on a solid surface [19]

The symbols γ are the surface energies of the liquid/solid, liquid/vapor, and solid/vapor interfaces as illustrated in figure 2.13. If $\gamma_{SV} > \gamma_{SL}$, then θ contact angle will be less than 90°. This causes the drop to spread and wet the surface of the solid at a rate determined by the liquid viscosity and surface roughness [19]-[20].

There are two chemical bonds to consider. The first is wetting followed by any degree of dissolution. This chemical bond is an interaction of electrons of the atomic scale and is greatly hindered by the presence of oxide films. If a contact

angle between the two phases is less than 90°, then wetting can occur followed by dissolution. It must be noted that if the solubility of the reinforcement in the matrix is significant, then during processing or future heat cycles dissolution can alternatively deteriorate the reinforcement.

The second chemical bond is characterized by the formation of a new chemical compound at the interface by one or more chemical reactions. These bonds can be covalent, ionic, metallic, etc., and are frequently very strong. However it is often observed that the reaction is inadvertent or too strong, and has detrimental effects by forming reaction products detrimental to the composite strength. A plausible solution to create a strong chemical interface free of extensive dissolution and chemical reactions is to use a reinforcement which is chemically similar to the matrix [20] or a catalytic substrate that is in thermodynamic equilibrium with the matrix.

2.4 Theoretical approach of strengthening mechanism in the AMC

The most important role of the matrix in particle reinforced composite materials is to transmit load to the reinforcing particles [18]. Both matrix and reinforcement particles share the applied load. Hardening and strengthening due to particles in the composites occur initially when the dispersed particles restrict matrix deformation by mechanical restraint. The amount of the restraint is a

complex process and depends on structural factors. It is functions of the ratio of the particle separation distance to the particle diameter and the ratio of the elastic properties o f the matrix and the second phase.

2.4.1 Composite classification based on the size and distribution of the second phase component in the composite

The composite alloy developed in the present research fits on the classification type of particle reinforced aluminum matrix composites, where the composite contains a second phase as fine particles distributed randomly in the Al matrix. In general, the different types of microstructure that can be achieved leading to a classification system according to the particle size level as follows [18] :

- Nano-composites materials (particle size with diameter of d~10 to 100nm)
- Micro-composite materials (particle size with diameter of d~1 to 10μm)
- Macro-composites (d>100 μm) e.g. steel wire-reinforced aluminum alloys

2.4.2 Orowan strengthening mechanism

This theory is defined as resulting from obstruction of a dislocation line motion “through” a reinforcement particulate, and is observed in dispersion-and particle-strengthened composites. Dislocation lines move on closed packed

planes in closed packed directions, and reinforcement particulates will hinder the dislocation motion by absorbing energy through the formation of Orowan loops thus causing strengthening [20] as illustrated in figure 2.14.

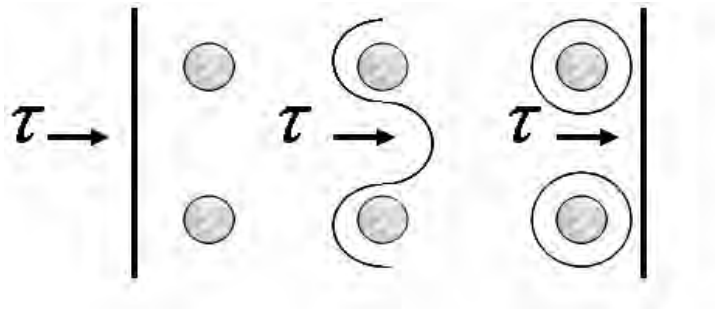

Figure 2.14 Orowan process of a dislocation bowing around a particle and leaving a dislocation loop [1]

The strengthening predicted by the Orowan equation $\sigma_{c,ds}$, is given by [21],

$$\sigma_{c,ds} \cong \sigma_0 + \frac{3Gb}{L_{e-e}} \qquad \textbf{(2.3)}$$

where $L_{e\text{-}e}$ is the interparticle spacing variable and is the edge-to-edge reinforcement spacing. G is the elastic shear modulus of the matrix; b is the magnitude of the matrix Burger's vector. $\sigma_{c,ds}$ is the flow stress of the composite, and σ_0 is the associated flow stress of the matrix. Equation (2.3) predicts $\sigma_{c,ds}$ reaches infinity as $L_{e\text{-}e}$ approaches zero.

The Ashby-Orowan equation is a modification to the Orowan equation that takes into account a minimum reinforcement size of an atomic diameter. If the reinforcement size is too small, it becomes a solute atom and loses its ability to provide strengthening by interacting with dislocations in an incoherent manner. The dislocation core radius, r_0, is the scaling term in equation (2.4) which identifies when strengthening by Orowan loops no longer exists for a particle of size d_r. The dislocation core radius in the Ashby-Orowan equation is physically the size of the dilated lattice under a dislocation, where a solute atom could be located. The strengthening contribution as predicted by the Ashby-Orowan equation for polycrystalline particle-hardened systems is :

$$\Delta\sigma = \frac{2.4Gb}{2\pi(1-v)^{0.5}} * \frac{\ln(d_r / r_0)}{L_{e-e}} \qquad \textbf{(2.4)}$$

Where d_r is the reinforcement diameter, r_0 is the dislocation core radius, and v is the Poisson's ratio of the matrix [21],[15].

The above theory is relevant to be considered in the present research as the way to complement the understanding which causes the strengthening and hardening in the composite.

3 PROCESSING METHODOLOGY FOR THE SYNTHESIS OF (AlMg)B_2 – ALUMINUM BASED COMPOSITES UNDER VACUUM

The present chapter describes a novel processing route to incorporate MgB_2 into an Al matrix. The methodology implemented promoted the necessary reaction for the formation of composite containing (AlMg)B_2 using Al pellets and MgB_2 powder as starting materials.

Initial experimentation could not achieve the incorporation of MgB_2 into aluminum because of the lack of wettability between both components. Aluminum high surface tension and oxide layer (Al_2O_3) formation most likely prevented magnesium diboride from mixing with liquid aluminum.

In the first attempt 90%Al pellets and 10%MgB_2 powder were heated in an evacuated quartz tube at high temperatures (1000-1200°C) without any visible reaction. A carved cylinder of Al 99% was filled with MgB_2 powder at 950ºC for 2 hours; yet, in this second case no reaction was present.

Later, the high energy ball milling process was incorporated in the process to reach the mechanical alloying Al and MgB_2. Many previous tests were necessary to

determine appropriate milling time, rpm and impact parameters, as well as number and diameter of the balls.

The mechanical alloyed samples obtained via ballmilling, were pressed and compacted into several coin shapes to facilitate sample analysis. During the melting process the compacted pills were placed into evacuated quartz tubes that were sealed later on. Figure 3.1 shows the experimental process designed to obtain the alloy.

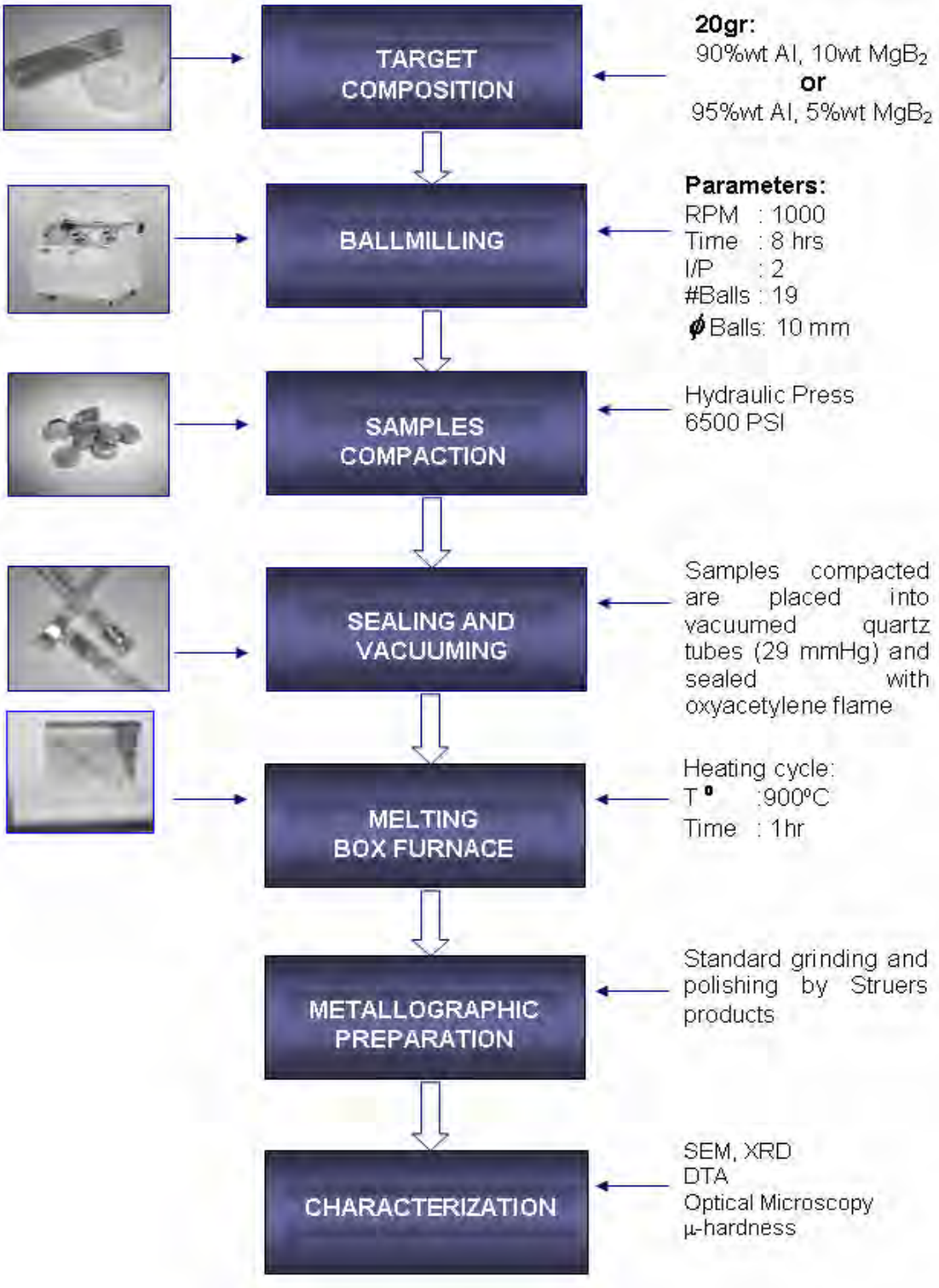

Figure 3.1 Squematic sequence of the experimental process designed

3.1 Step of ball milling process

Ball milling variables and its influence in the final results of the mechanical alloy were explained in the chapter 2. A Vario-Planetary Ball Mill Pulverisette 4 Fritsch™ was used for mechanical activation and alloying. High energy ball milling experiments were conducted on 325 mesh (44μm) MgB_2 and aluminum pellets (841-2380μm).

A set of previous experiments with several samples were ball milled varying the operation parameters until optimal levels were found:

- A range of ballmilling times combined with low to high rpm was tested. The results of the two extreme cases were:

    - At a short milling time of 5 hours at 500 rpm no mixing was found between Al and MgB_2. MgB_2 stuck onto the balls and jar walls but aluminum did not.
    - Long milling time of 15 hours at 1200 rpm promoted the cold welding of the entire charge composition (Al and MgB_2) into the jar walls and balls; in this case the alloying material could not be recovered. Further treatment with diluted sodium hydroxide was needed to remove the aluminum from the inner walls of the container.

- Three different ball diameters were tested to analyze their optimal performance. The number of balls was varied to find the proper ball to powder weight ratio, BPR. The best routine was obtained with 19 balls with diameter of 10 mm.

Table 3.1 shows the configurations with respect to number and diameter of balls used in the preliminary runs. For simplicity no combinations of small and large balls were used to randomize the motion.

Table 3.1 Balls configurations for the previous runs

Number of Balls	Diameter of balls (mm)	Total ball mass (g)
40	5	20
19	10	76
8	15	198

- After number of balls and their diameter were selected, the charge weight of Al + MgB_2 to be milled was set to ensure at least 50% empty space volume in the container that guarantees proper balls movement.

- The jar capacity used was 45cm^3 and the total balls volume (19 units of 10mm diameter) was 0.52 cm^3. The volume for the charge composition (Al+MgB_2) was

7.38cm^3. The empty free space in the jar was 82%. This provides enough space for ball movement. The ball-to-powder weight ratio BPR was 4:1.

- Three different aluminum sources were used to prepare (AlMg)B_2 composites. In previous runs with Al chunks, Al pellets and Al powder were mixed with 44μm elemental MgB_2 powder, to determine the best wettability state between the charges component (Al+MgB_2) in the ballmilling process. Table 3.2 shows some cycles implemented in those tests. Large aluminum shots inhibited good balls motion and no interaction between the charge components was noticed (figure 3.2. b). Also the shape of many Al shots did not change after milling. In the run processing with Al powder there was cold welding in the jar inner walls. The best performance (less cold welding occurrence) and wettability was obtained with Al pellets (figure 3.2.c). This prompted the selection of these variables for the remaining work of this investigation.

Table 3.2 Ball milling cycles implemented varying Al particle size

Sample composition	RPM	Time (hr)
Al chunks (4500-5000μm)+ 44μm MgB_2	1000	10
Al powder (149-44 μm)+ 44μm MgB_2	800	8
Al pellets (2380-841μm)+ 44μm MgB_2	800	8

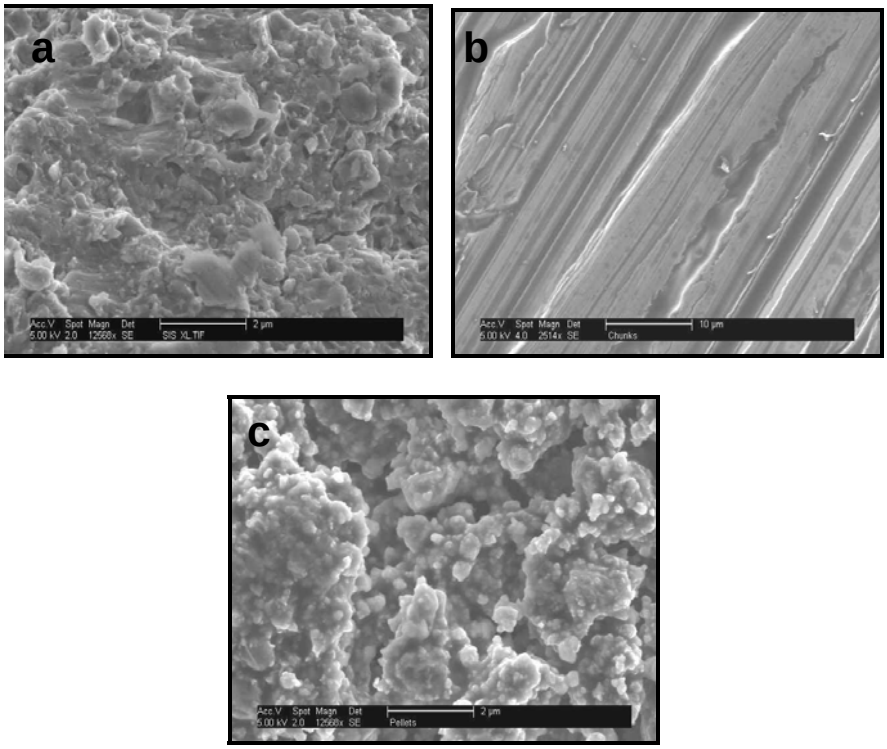

Figure 3.2 SEM images at 2μm wettability behaviors with MgB_2 varying Al mesh. (a) Al powder (cold welding) (b) Al shots (not mixing)(c) Al pellets (good mixing)

- The preliminary runs were developed in two different materials for grinding medium, tempered steel and tungsten carbide. All final experimentations were done with the tempered steel jar and balls. At the time we have only one WC jar. For balancing in the main disk it was recommended to use the same weight and size of jar.

After selection of the above parameters and running several tests in the ball milling machine, three sets of cycles for milling time and rpm were chosen: low, medium and high as shown in the table 3.3. Combining rpm and milling time led to nine different experiments. The charge composition (90%Al, 10%MgB_2) and impact parameter (-2) were kept constant in all cases to facilitate experimentations. A design of experiment was implemented to find appropriate parameters that would lead to optimal mixing.

Table 3.3 HEBM test parameters

Cycle	Milling time hr	RPM
LOW	6	600
MEDIUM	***8***	800
HIGH	10	***1000***

In the cases of low cycles (6 hours at 600, 800 and 1000 rpm) of processing one could observe poor mixing between components. Free MgB_2 powder remained covering aluminum pellets, inner walls of the container and was stuck onto the balls too. With medium cycle (8 hours at 600 and 800 rpm) the mixing improved; yet, a large quantity of loose MgB_2 powder was covering the Al pellets. Figure 3.3 (a) shows MgB_2 covering just the perimeter of Al pellets without reaching the inner area. At a high cycle of 10 hours cold welding started to appear, causing material loss and the corresponding difficult to remove it from the grinding media.

As indicated in chapter 2, milling time is one of the most important parameters to achieve equilibrium between mixing and cold welding to subsequently facilitate the alloying. Therefore a combination of medium cycle in time of 8 hr and a high cycle of 1000 RPM produced the best mixing or mechanical alloying.

Figure 3.3 (b) shows a pellet with appropriate mixing where the MgB_2 is present around and within pellet. To minimize oxidation of MgB_2 powder, a portable glove box was employed to weigh and mix this powder with the Al pellets in the selected proportions under an argon atmosphere.

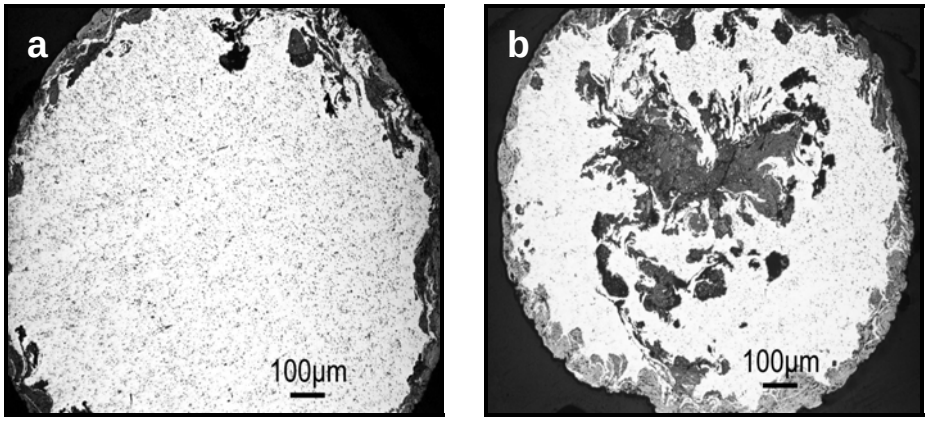

Figure 3.3 Al pellets with MgB_2 at 50X after ballmilling. (a) Poor mixing, MgB_2 remains just around pellet (b) Appropriate interaction and mixing between components

3.2 Step for samples compaction

The mechanically alloyed composite has both spherical and flattened particles. To facilitate the handling of the alloy during the melting and characterization steps the material was compacted at 6500 psi obtaining coin-shaped specimens of 10 mm diameter. (Figure 3.4a)

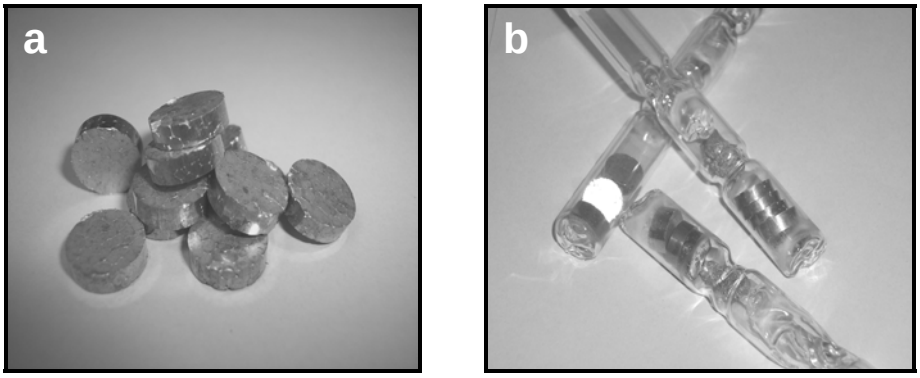

Figure 3.4 (a) Samples compacted after ball milling (b) Evacuated and sealed quartz tubes

Samples were processed under two different compositions of Al+MgB_2 composites: 5-10wt% MgB_2. A ductile-brittle mechanical alloying was obtained.

3.3 Step of vacuum evacuation and sealing of quartz tubes

After the material compaction, a set of 6 samples coins was introduced into each 15 cm length quartz tube. The quartz tube diameter was reduced from 12 mm to 4 mm, in order to separate into two connected chambers where the samples and a piece of titanium sponge were introduced. Titanium sponge acted as oxygen getter to minimize sample oxidation. Afterwards vacuum the quartz tube (with the sample and titanium sponge) for 5 minutes was required to protect the samples from further oxidation during melting. The Laboport vacuum pump used delivers 29 inHg. Finally, the quartz tube was sealed using an oxyacetylene flame (figure 3.4 b). A blue flame with short length was strong enough to heat and seal the tube.

3.4 Step of melting process

In the preliminary experiments to melt the mechanical alloying, an arc melting furnace, MRF was employed. This method was later abandoned due to the observed Mg high vapor pressure that caused its volatilization during arc-melting because of the temperatures reached during the operation.

Metallographic and SEM/EDS analysis revealed Mg depletion throughout the arc melted samples (figure 3.5). Furthermore, the shape of AlB_2 reinforcements obtained was needle-like due to the high solidification rates.

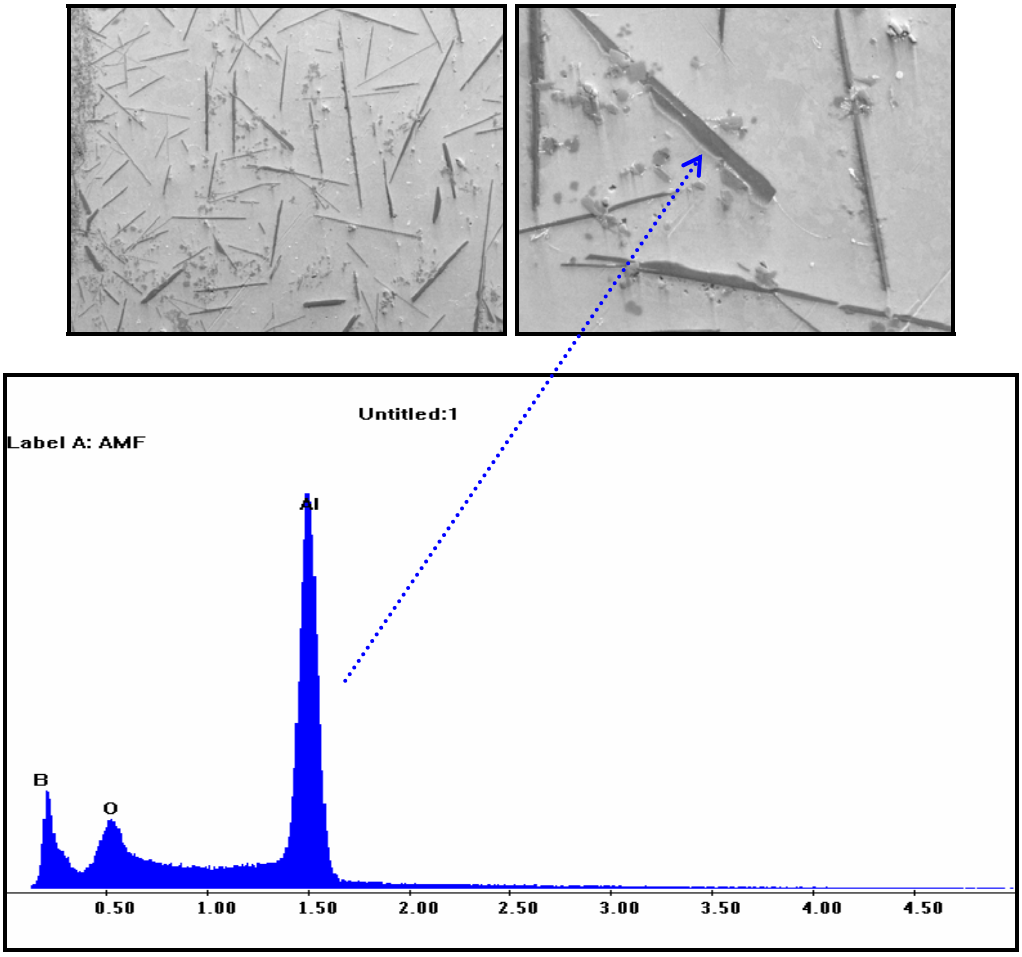

Figure 3.5 Backscattering Electron Image (2000X)-EDS Spectrum (ACCV 5kV)

As a consequence, an electrical resistance box furnace was used for the melting of the samples sealed in the evacuated tubes. A set of three tubes with the

selected compositions were placed inside the furnace at 900ºC for one hour to allow the melting of the Al matrix.

3.5 Metallographic sample preparation

A sample surface free of scratches is necessary for optical microscopy, and SEM analysis. After mounting samples in epoxy, BUEHLER® α and β grinder and polisher were used for the sample preparation. The grinding steps included SiC papers with 400, 600 and 800 grits. For the polishing process a 3μm diamond Struers® DP suspension was utilized on a Struers® MD-MOL short felt cloth. Final polishing was carried out with a Struers OPS SiO_2 (0.05μm) emulsion over a Struers® MD-CHEM short felt cloth. An ultrasonic cleaner helped eliminate cross contamination on the samples. All samples were viewed in a NIKON EPIPHOT 200 inverted optical microscope. The characterization process of the prepared samples obtained in this step is explained in the next chapter.

4 CHARACTERIZATION OF (AlMg)B_2 –ALUMINUM BASED COMPOSITES AND NANOCOMPOSITES

Latest progress in the studies of bulk amorphous, quasi-crystalline and nanocrystalline alloys has resulted in significant improvements in the strength of Al-based alloys. Several of these Al alloys derive their superior strengths from either a microstructure of nanoscale FCC Al crystals distributed in an amorphous matrix or a microstructure containing a mixture of nanoscale FCC Al particles and intermetallics compounds. However, in some cases, the superior strength comes from a mixed microstructure of crystalline nanoparticles distributed in a continuous FCC Al matrix [22]. The composite studied in this research had a mixed microstructure of crystalline particles and nanoparticles of (AlMg)B_2, distributed in a continuous Al phase and Al_3Mg_2 + Al eutectic.

The preceding chapter explained the development of a process for the synthesis of (AlMg)B_2 composite starting from ballmilling, followed by samples compaction and the melting under vacuum in an electrical resistivity furnace. This chapter describes the characterization of the samples bearing two different compositions (Al-5%wtMgB_2, Al-10wt%MgB_2). Quantitative microstructural characterization was completed with Image J software version 1.34s public domain. Scanning electron microscopy (SEM) was used to measure the nanosized reinforcements and the composition of the reinforcements. Vickers microhardness was measured for both matrix and reinforcement. XRD and DTA were also used to

corroborate phase formation. As a complementary part a crystallographic model of the ternary (AlMg)B_2 phase is presented at the end of the chapter, and developed using the CARIne® crystallographic package version 3.1 software.

4.1 Microstructural characterization

Characterizing the microstructure of an alloy is a science in itself and in fact is the most important of this entire subject area. This section will analyze the morphology (size and shape) and the volume fraction of the reinforcements present in the (AlMg)B_2 composite. Stereology assisted by analysis was used to estimate the average of particle size and volume fraction using the IMAGE J® software.

4.1.1 Microstructure

The most important part of this, was the visual recognition of the expected phases in the (AlMg)B_2 composite and its distribution in the Al Matrix, based on the phase diagrams presented in chapter 2. This analysis was conducted using a NIKON EPIPHOT 200 inverted optical microscope. The ensuing microstructure is presented in the figures 4.1 and 4.2. Figure 4.1 (a) shows the reinforcement embedded in the aluminum matrix for the Al-10wt%MgB_2 composite. Figure 4.1(b) illustrates the eutectic Al_3Mg_2 + Al, being one of the stable phases in the binary system Al-Mg. Figure 4.2 presents both eutectic and reinforcement particles (large and nanometer-sized ones).

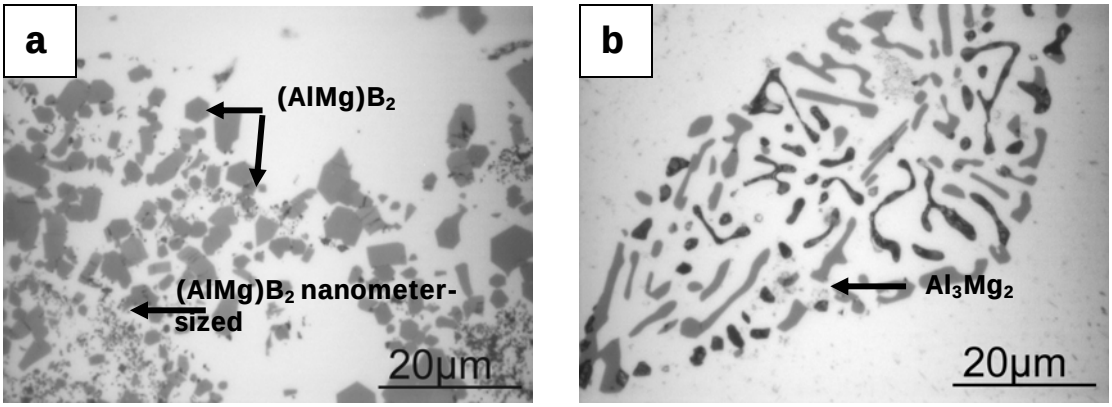

Figure 4.1 (a) Micrograph of Al-10wt% MgB_2 composite showing both reinforcements sizes large and nanometer-sized (1000X) (b) Microstructure Al-5wt% MgB_2 composite showing eutectic phase (1000X)

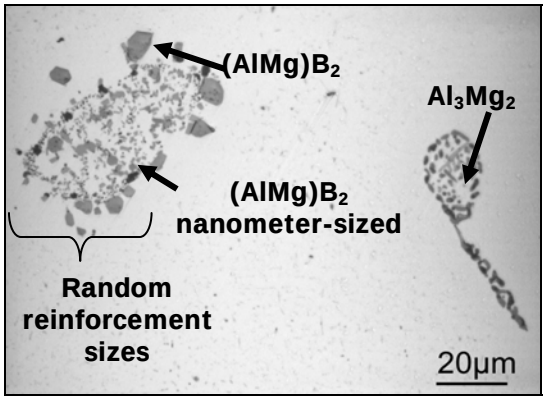

Figure 4.2 Microstructure Al-10wt% MgB_2 composite showing corresponding phases embedded in the Al matrix and different reinforcement sizes (500X)

The practical insolubility of boron in the Al matrix allows combining the high hardness of the AlB_2 reinforcers into the soft and low density of the aluminum matrix. Furthermore, the aluminum diboride has a density of 3.19 g/cm^3 [2] which is 26,7% more than liquid aluminum. Reinforcement particles $(AlMg)B_2$ are also apparent and

its chemical composition was determined in the SEM analysis by EDS as explained below.

4.1.2 Reinforcement particle size

The reinforcement particles found in the two different compositions (Al-5wt %MgB_2, 10wt%MgB_2) differed in size and shape requiring a more detailed study of the distribution of both size and shape of reinforcement. This wide range of shape and size was probably caused by the ballmilling process used to achieve the mechanical alloying.

In order to describe the particle size distribution (PSD) of the composite, a filter range of eleven size fractions (0.10 to 4.52 μm) was chosen out to be counted and evaluated by using the "analyze particle" option provided by the IMAGE J® program. No apparent differences between compositions after 1.4 μm particle size were observed; similar amounts of particles were found with sizes from 1.4 to 4.52μm in the two compositions. Figure 4.3 presents a histogram of the particle size for both compositions Al-5wt%MgB_2, 10wt%MgB_2 within the range 0.10 to 4.52 μm.

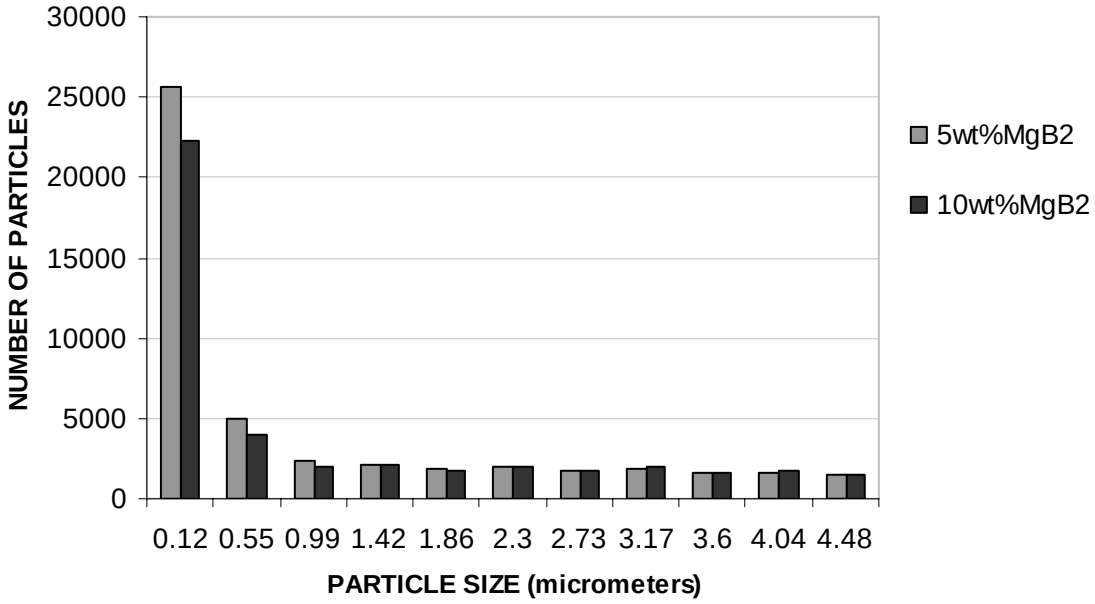

Figure 4.3 Frequency histogram of particle size distribution

The Al-5wt%MgB_2 composite shows relevant higher amount of smallest particles sizes (0.12 -0.55μm) frequency. This will be corroborated in 4.1.4 where this parameter led to the higher values of HV in the composite. Less amount of MgB_2 conducted to more reduction of the powder particles in to the grinding medium. As the reinforcement particle size is smaller occurs a rising in the number of dislocations promoting higher strength in the composite.

There is no pattern in the grouping followed by the different particle sizes for both compositions. This trend is predictable since the ballmilling process implemented generates thousand of fractures randomly forming a large number of interfaces between the composite milled (explained in chapter 2). The composite developed corresponds to an AMC with non continuous reinforcement particles.

Figure 4.4 represents the histogram distribution for the whole particles sizes (0.2-23μm) as measured using the IMAGE J software for the composite.

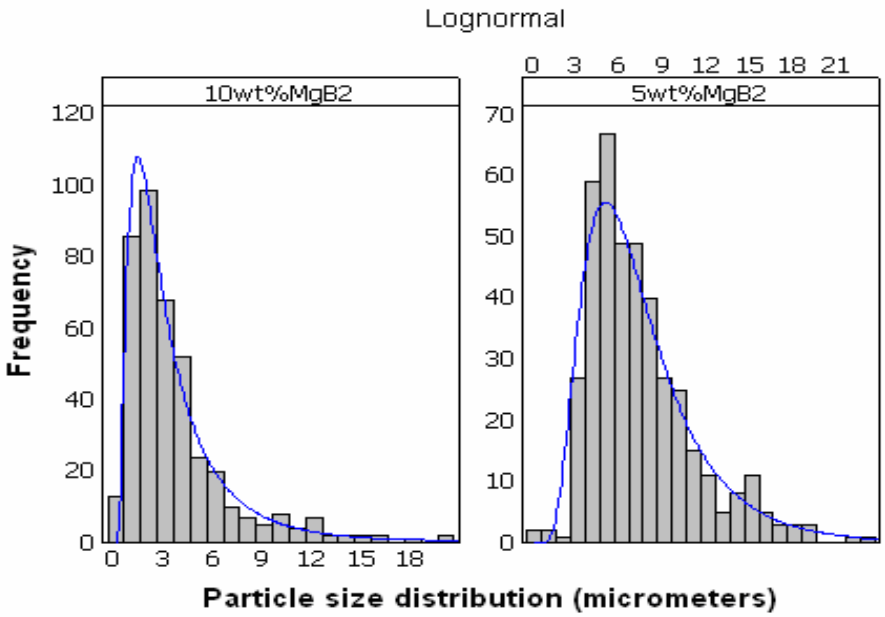

Figure 4.4 Frequency histogram of particle size distribution for each composite

The data in figure 4.4 follows a lognormal distribution with 3.6μm mean particle size and 3.23 stdev for samples containing 10wt%MgB_2 and 7.33μm mean particle size and 3.69 stdev for samples with 5wt%MgB_2. Appendix C1 display details this analysis. Furthermore, figure 4.5 shows the average particle size for each composite alloy.

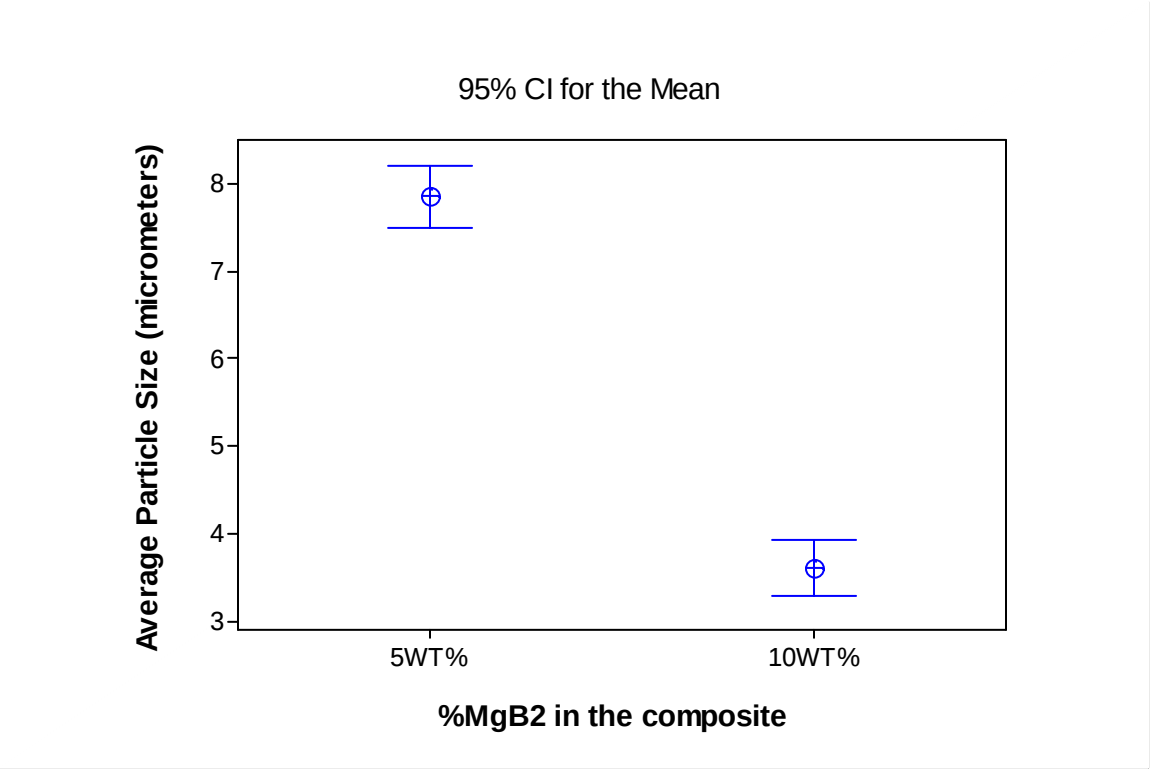

Figure 4.5 Particle size vs. wt%MgB_2 for composites

4.1.3 Volume fraction of reinforcements

To quantify volume fraction in the composite alloys, micrographs at 200X-500X magnification were used for the measurements with the IMAGE J® program. Examples of those micrographs quantified by volume fraction are shown in figure 4.6.

The presence of many large particles and the smallest or nanosized ones indicates a two different ranges of size distribution (micrometric and nanometric) produced in the step of ball milling process due to the ball-particle-ball collisions, which cause the particle to fracture thousand times. Figure 4.7 presents a plot for the reinforcement volume fraction of the composites, where no relevant difference in the values was found.

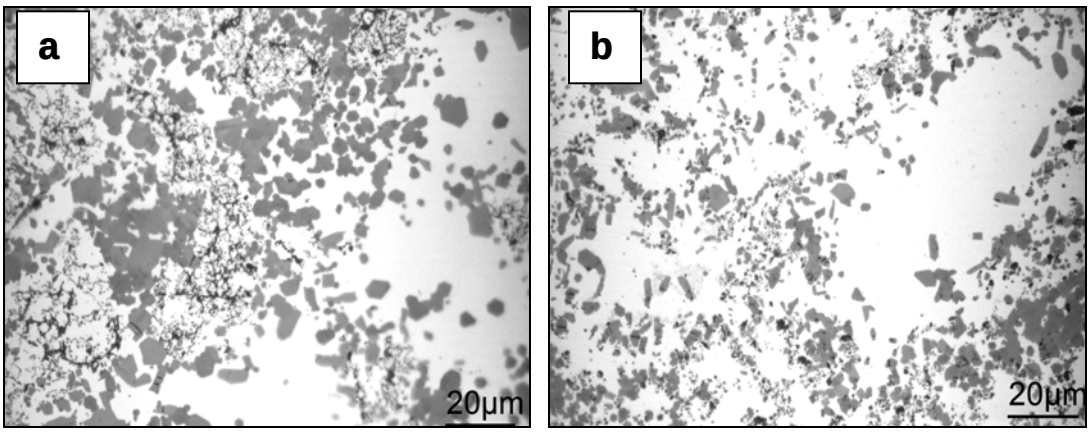

Figure 4.6 (a) Micrograph for Al-10wt%MgB_2 alloy, 24.2% volume fraction (500X) (b) Micrograph for Al-5wt%MgB_2 alloy, 21.8% volume fraction (500X)

The volume fraction average in the composite with 10wt%MgB_2 is 23.73% with 8.88 StDev, while for composition 5wt%MgB_2 the mean of volume fraction is 22.44% with 7.66 StDev. Appendix C2.

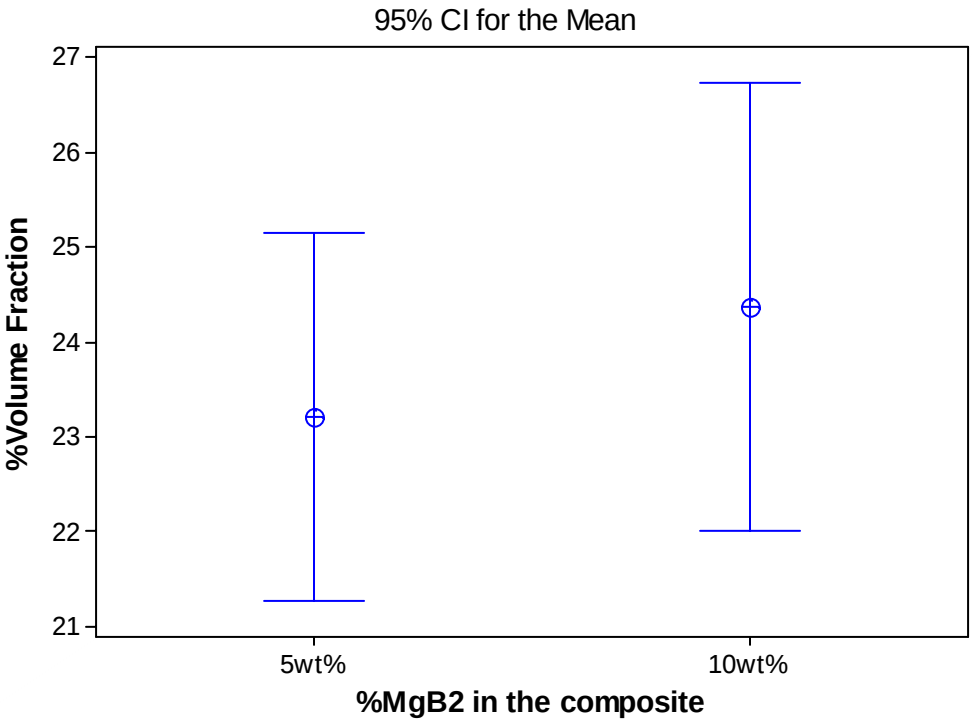

Figure 4.7 Reinforcement Volume fractions for both compositions

Figure 4.8 presents the probability plots for the composite alloys. The data fits better in a Weibull distribution for the 5wt%MgB_2 composition.

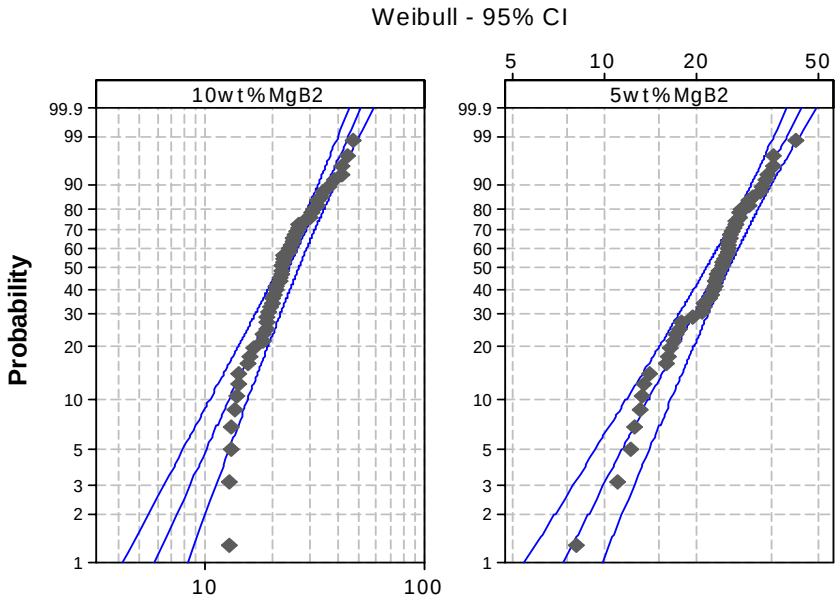

.

Figure 4.8 Volume fraction probably plots for both composites

4.1.4 Vickers microhardness measurement on the reinforcements and matrix

A Buehler-Micromet®II hardness tester was used to perform the microhardness measurement on the composite samples. The Vickers hardness test method consists of indenting the test material with a square-based pyramid diamond indenter and an angle of 136^{o} between opposite faces. The two diagonals of the indentation left in the surface of the material after removal of the load are measured using a microscope. Equation (4.1) shows the calculation for Vickers hardness [23]:

$$HV = \frac{2F\sin\left(\frac{136^o}{2}\right)}{\left[d^2\right]} \approx 1.854\frac{F}{d^2} \quad \textbf{(4.1)}$$

F Load in kgf
d Arithmetic mean of the two diagonals, d1 and d2 in mm
HV Vickers hardness

The ASTM E 384-99 indentation hardness of materials can be referenced in this test. A 25gf (HV_{25}) load was applied for a period of 15 seconds to perform the test in the (AlMg)B_2-based composites. Vickers microhardness data were obtained from a number of polished samples of Al-5wt%MgB_2 and 10wt%MgB_2 composites.

Vickers microhardness of the reinforcement and the corresponding volume fraction of the surrounding area were studied. The range of microhardness recorded started from 57.1 to the highest value registered at 361.95 HV, with 12.6% to 44.8% volume fraction values respectively. Figures 4.9 and 4.10 present the results of this study. The HV measured on the composite samples varied greatly and the data is too widespread. The first three micrographs in figure 4.10 are before indentation and the corresponding indented ones are below each one of the three first presented.

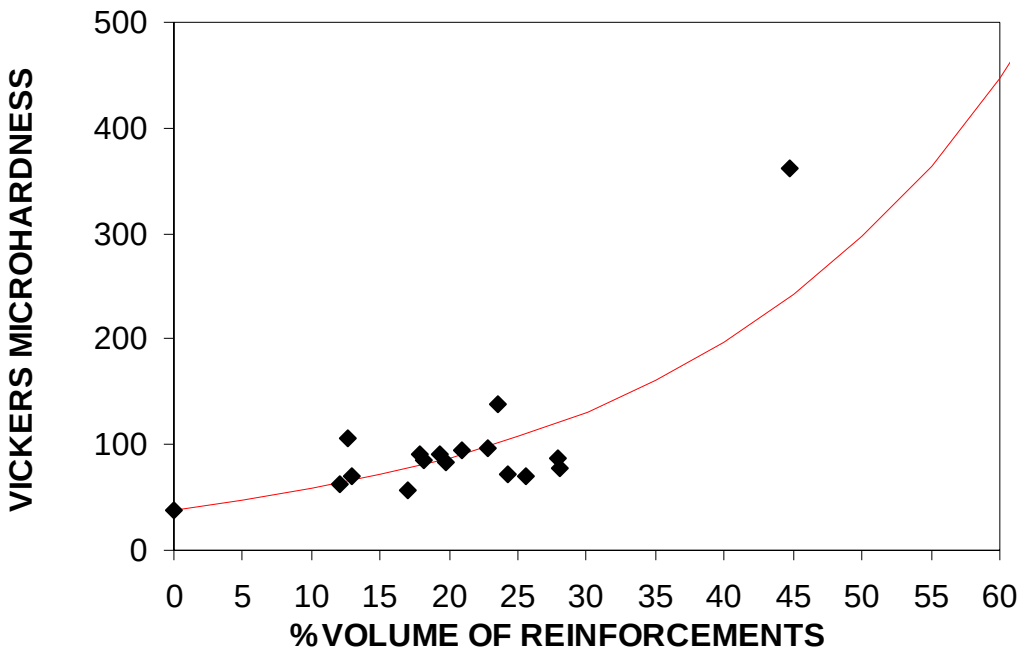

Figure 4.9 Reinforcement microhardness vs. %Volume of reinforcement area

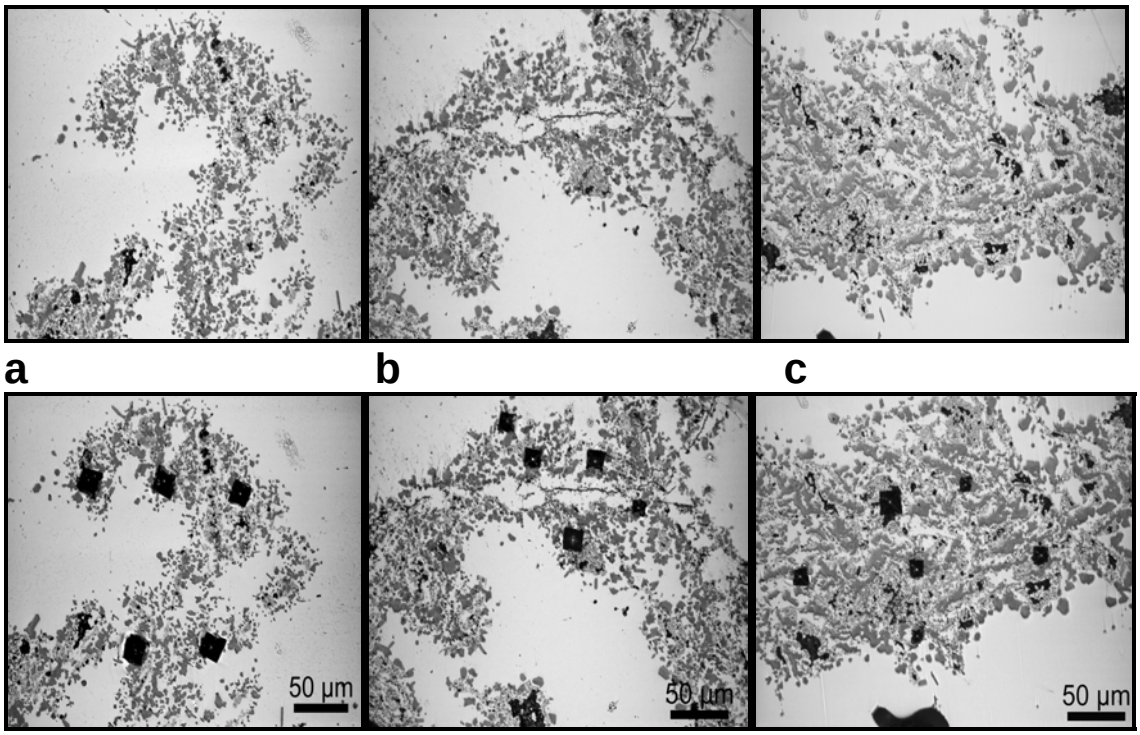

Figure 4.10 Micrographs reinforcements indented by Vickers microhardness (200X) (a) Vol.fract 22.8%, 86.4 HV, Al-5wt%MgB_2 (b) Vol.fract 17%, 57.1 HV, Al-5wt%MgB_2 (c) Vol.fract 27.9%, 97.18 HV, Al-10wt%MgB_2

The Vickers microhardness was also measured on the matrix (figure 4.11) for the both compositions studied. A high average of matrix hardness was found in samples with 5wt%MgB_2. As presumed before, larger amounts of nanometer-sized reinforcement particles were present in this composition; the nanoparticles sizes has direct influence in the hardness parameter due to the strengthening promoted by increasing the number of dislocations after plastic deformation in the indented area

as explained in the Orowan strengthening mechanism (2.4.2). Furthermore, dispersed nanoparticles restrict matrix deformation by mechanical restraint [18]. Also, the microhardness in the matrix is being affected by the presence of reinforcing particles in the subsurface.

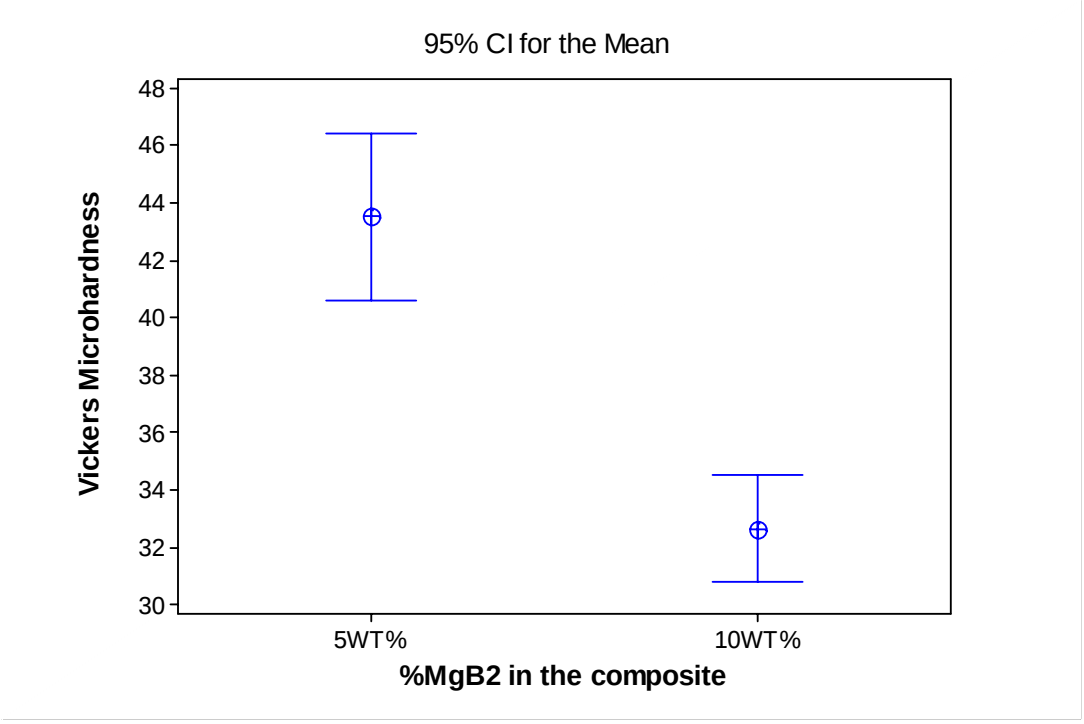

Figure 4.11 Matrix microhardness for 5wt%MgB_2 and 10wt% MgB_2 composites

The highest average of matrix hardness was found in the 5wt%MgB_2 composite (figure 4.11). The mean hardness for 10%MgB_2 composition is 32.65HV with a StDev of 7.05, while for 5%MgB_2 the mean is 43.53 and the StDev is 11.03. Appendix C3 presents details.

The figure 4.12 presents a plot using the data found in both compositions (5wt%-10wt%MgB_2) of reinforcement particles Vickers microhardness vs average particle size around the indented area. The result shows that higher values of HV were found for indented areas with the smallest particle sizes. The black trend line corresponds to fitting equation $HV=109.26(Part.Size)^{-0..5}$. The diamond points represent the measured data.

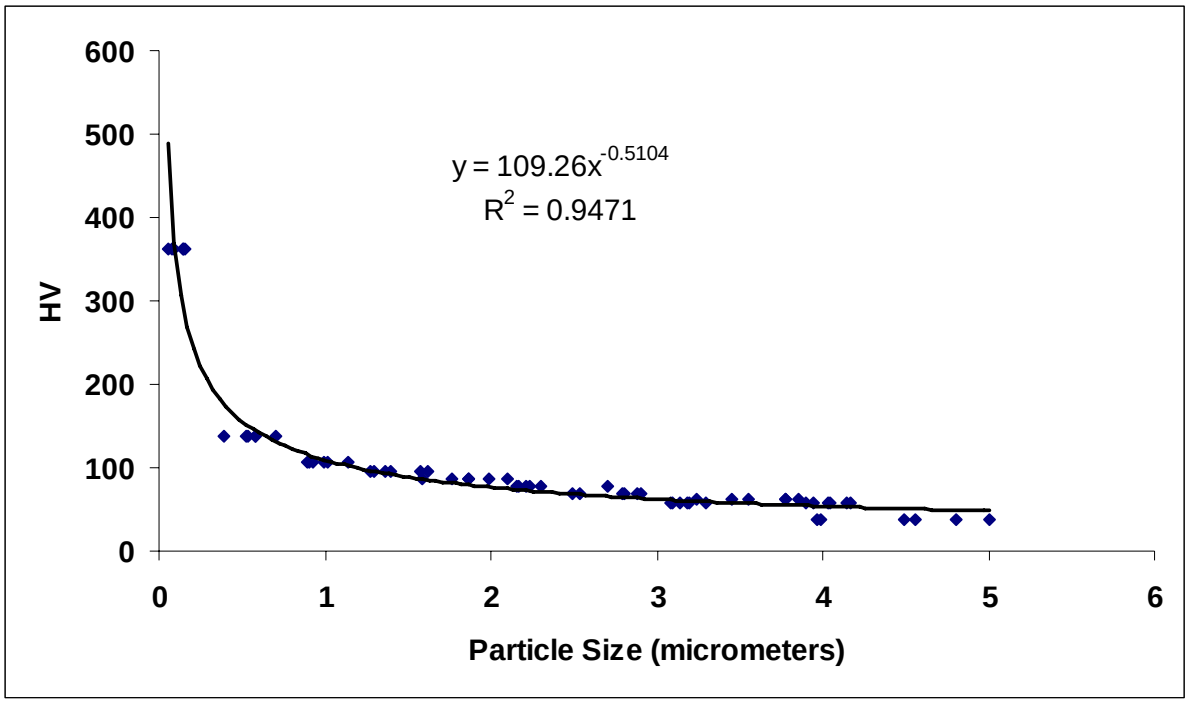

Figure 4.12 HV vs. Particle size using data of both compositions

4.2 Complementary Tests

4.2.1 SEM/EDS Analysis

In the $(AlMg)B_2$ composite the reinforcements particles are no longer spherical because they have been fractured rewelded and refractured a multitude times to generate the nanostructured size. This process has caused the particles to become asymmetrical and hexagonal like-shaped. Figure 4.13 presents six SEM images where the morphology and the dissimilar sizes of the reinforcements can be appreciated. Particle sizes down to 100nm were found in the SEM images as seen in figure 4.14.

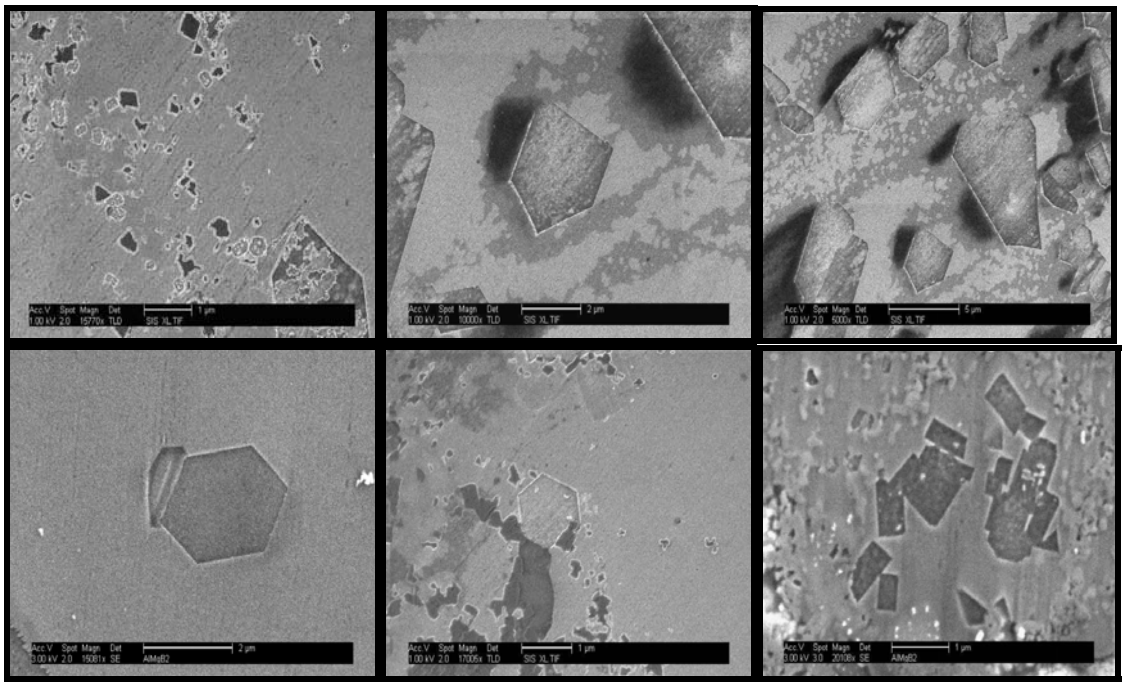

Figure 4.13 SEM images of morphology and dissimilar sizes of reinforcements

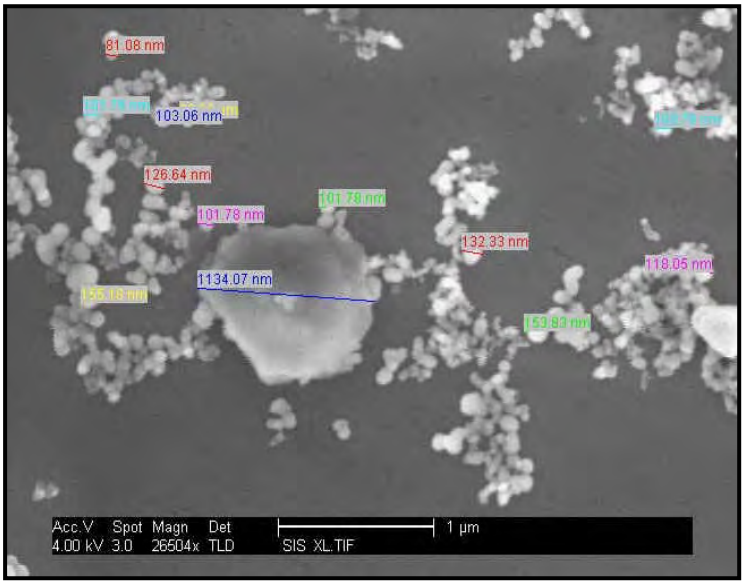

Figure 4.14 SEM image of several sizes of reinforcement particles

Figures 4.15 and 4.16 present the EDS analysis that helped to identify the elemental composition of the reinforcement particles. The three elements Al-Mg-B, are being part of the 200nm particle in figure 4.15. In addition, figure 4.16 (c), shows an EDS mapping corroborating the ternary system in the reinforcement particles achieved in the implemented process.

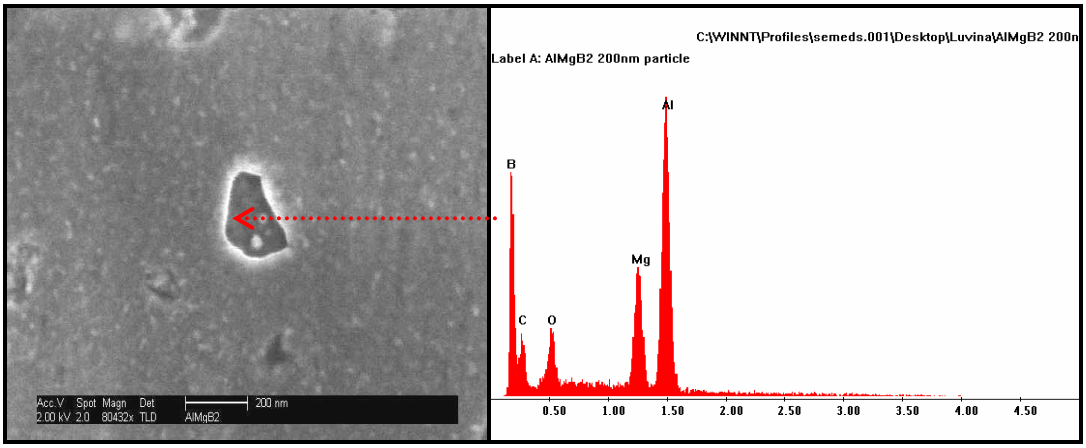

Figure 4.15 SEM image of (AlMg)B_2 reinforcement at 200nm and its corresponding EDS

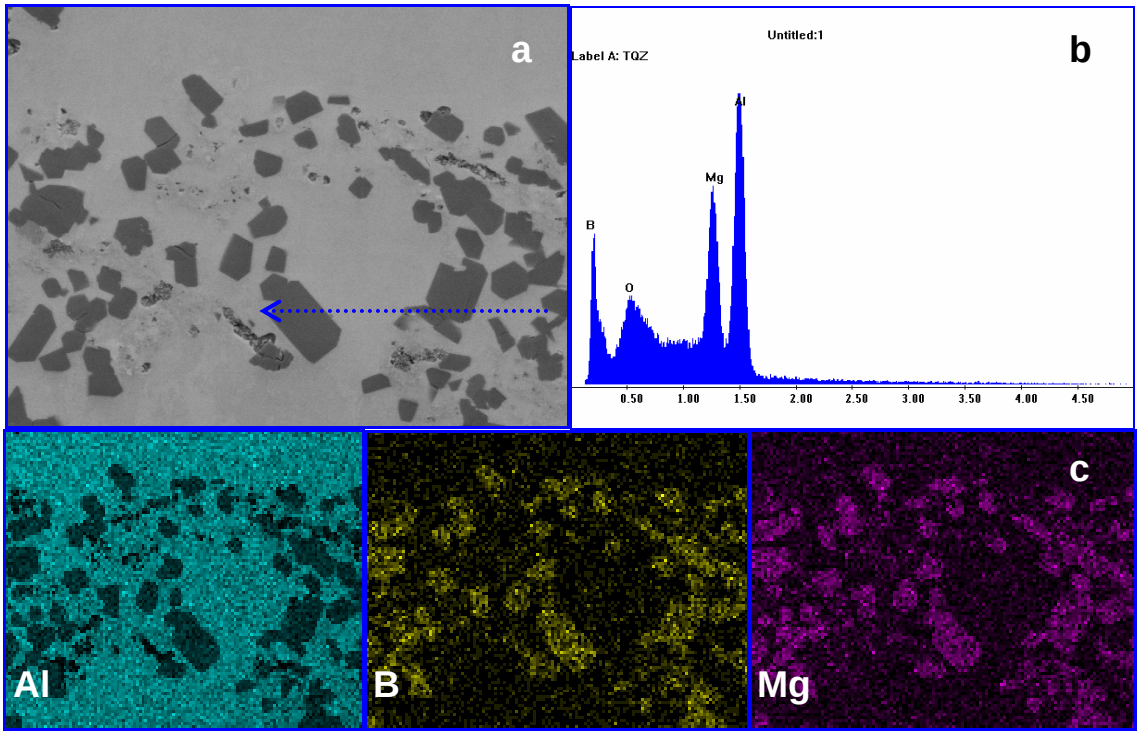

Figure 4.16 (a) Backscattering Electron Image (2000X) (b) EDS spectrum (5kV) (c) EDS maps

4.2.2 X Ray Diffraction Analysis

Phase identification in the composites was carried out by X-ray diffraction (XRD) with a SIEMENS D500 diffractometer (Cu Kα radiation) with 2 sec. steps of 0.02° of 2θ diffraction angle at 40mA and 40kV. Both composites (Al-10wt%MgB_2 and 5wt%MgB_2) were investigated in the solid and powder form at room temperature. Diffraction patterns were obtained and then analyzed using MATCH® software [24].

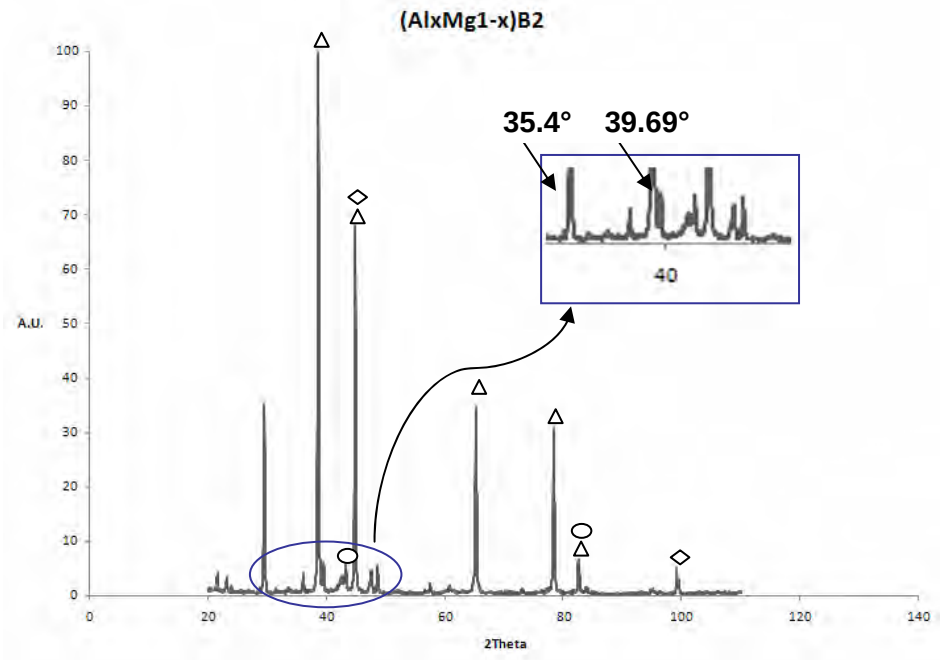

Figure 4.17 XRD patterns for Al-10wt%MgB_2. Al△, MgB_2○, AlB_2◇

The identified phases found in the micrographs in figure 4.1 (a) and (b) were also present in the XRD diffractogram in figure 4.17. There is one evident MgB_2 peak, which indicates that not all MgB_2 particles have substitutionally dissolved Al atoms. There are small peaks between 20^o to 45^o that appeared around AlB_2(101), Al(100)(111)(200), and MgB_2(101) peaks and are associated with the ternary $(AlMg)B_2$ phase.

4.2.3 Differential Thermal Analysis (DTA)

This technique can be used to detect the physical and chemical changes which are accompanied by a gain or loss of heat in a material as its temperature is increased, decreased of held isothermally. A six milligrams sample in crucible of 30µl was used for this analysis in a N_2 atmosphere. The heating cycles were carried out at 5^oC/min from 25^oC to 950^oC, followed by a cooling cycle from 950^oC to 25^oC at 5^oC/m. A melting reaction was found at 618^oC (fig. 4.18). The dome showed at 820^oC is probably the dissolution of the ternary $(AlMg)B_2$ phase.

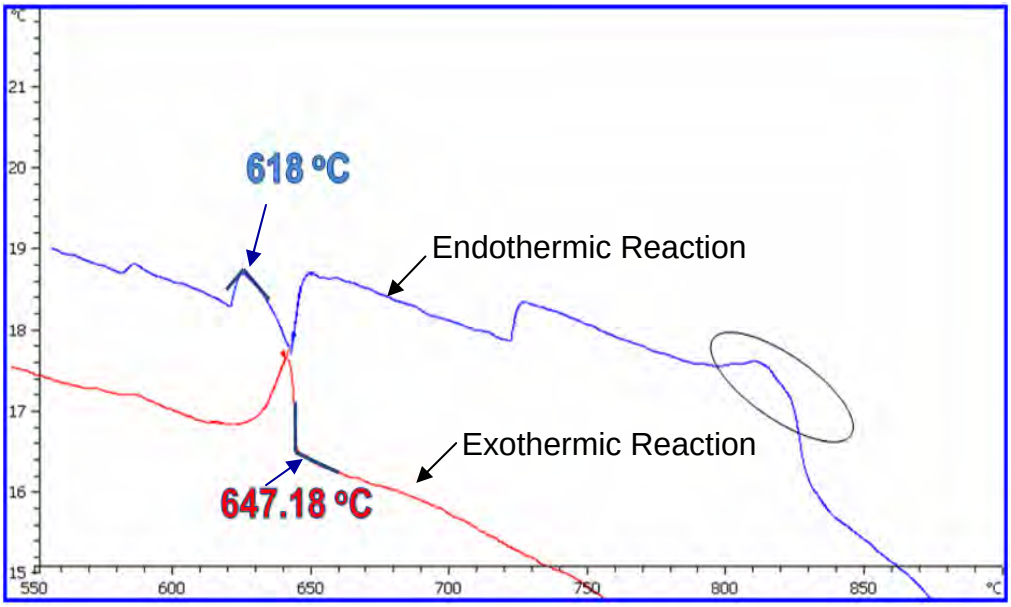

Figure 4.18 DTA ∆°T vs. °T curve for Al-10wt%MgB_2 composite

4.2.4 Density Calculations

Composite densities were calculated by theoretical and practical methods. Theoretical density for both compositions was calculated using the rule of mixtures (ROM) [18] indicated in equation 4.2. The first term of the equation ***($\rho_{matrix}V_{matrix}$)*** was calculated considering both Al matrix and eutectic Al_3Mg_2 phase present on it. The average volume fraction used for calculation was: 22% for the 10wt%MgB_2 composition and 20% for 5wt%MgB_2.

$$\rho_{Theoretical} = \rho_{matrix}V_{matrix} + \rho_{reinforcement}V_{reinforcement} \qquad (4.2)$$

For samples containing 10wt%MgB_2 the corresponding volume fraction of Al_3Mg_2 was 15%, while for samples containing 5wt%MgB_2, the volume fraction of this eutectic phase was 11%. According to table 2.2, the density of Al_3Mg_2 is 2.37 gr/cm^3 [2],[10].

The practical density of the composite was measured with a picnometer using the Archimedes principle described in ASTM D792 “Standard Test Method for Density and Specific Gravity”. The densimeter operates by measuring its buoyant force when submerged in a liquid of known density.

Table 4.1 Comparative densities average

Material	**Density practical (Archimedes) gr/cm^3**	**Density Theoretical gr/cm^3**
Pure aluminum	*2.71*	*2.71*
AlB_2	-	3.19
$(AlMg)B_2$	-	**2.81**
Al-5%MgB_2	**2.576**	**2.70(ROM)**
Al-10wt%MgB_2	**2.540**	**2.68(ROM)**

Table 4.1 presents the average densities for both theoretical and experimental densities for Al-5wt%MgB_2 and 10wt%MgB_2 composites. Theoretical

densities calculations were higher than experimental. It is presumed that after samples compaction, free spaces remain in the coin-shaped samples forming air chambers. This factor must be considered to understand the difference between both densities (theoretical and experimental). Mg low density promotes the reduction in the entire composite since Mg has two thirds of aluminum density. The impact of magnesium additions in the (AlMg)B_2- based composites are both to provide solid solution strengthening and weight reduction to the alloy as seen in figure 4.19.

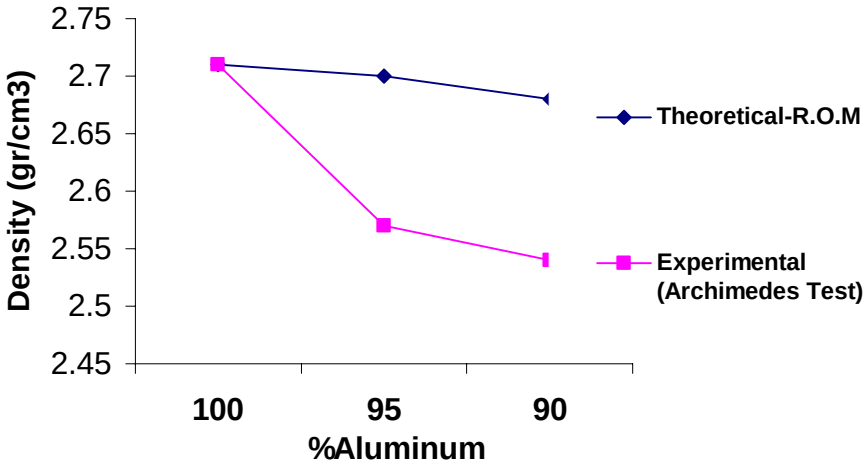

Figure 4.19 Calculated-theoretical and experimental densities vs %Al

Plot in figure 4.20 shows no significant differences between experimental densities data for the two compositions.

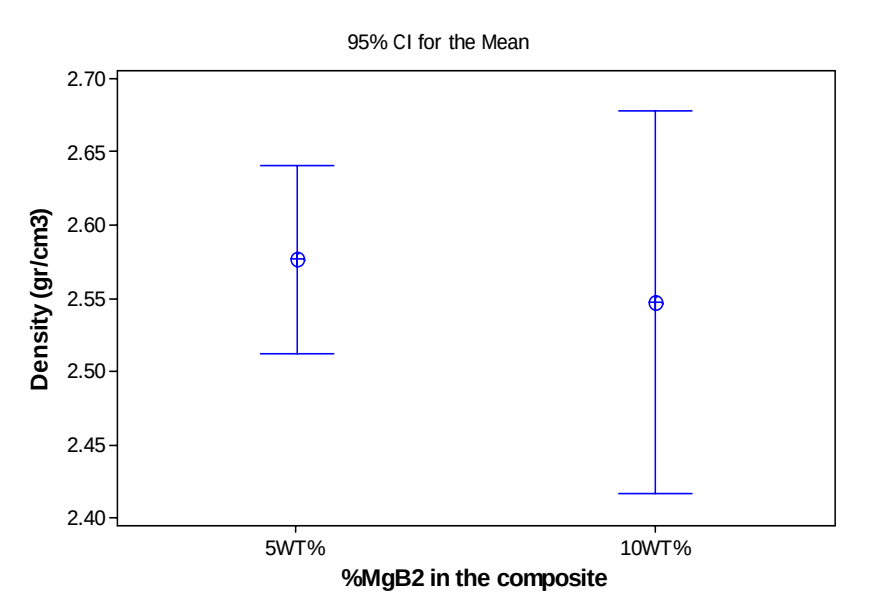

Figure 4.20 Experimental densities for both composites

4.3 Proposed crystallographic model of a composite bearing $(Al_xMg_{1-X})B_2$ phase

4.3.1 Simulation using CARIne Crystallography 3.1 software

Ternary phases such as aluminum-boron-magnesium have very little or no information available. The existing ternary phase diagram covers just 50at% of each element in the system.

Analysis via EDS and XRD evidence the presence of a ternary phase $Al_xMg_{1-x}B_2$. In order to determine a possible stoichiometric composition of that phase, a simulation using the CARIne crystallography software version 3.1 was implemented [25]. This simulation had two stages: first stage to build up a single crystal of the ternary composite and second stage to compare the output of the program, which is an XRD pattern with the XRD pattern from the actual samples.

For stage one, several crystals were created. The hexagonal Bravais lattice was decided to leave constant for all the simulations, since both AlB_2 and MgB_2 have hp3 configuration. The ball milling process itself introduced aluminum atoms to the MgB_2; the hp3 structure was used as the stepping stone for adding the atoms of aluminum or substituting the magnesium ones. The lattice parameters for these crystals were adjusted to give the best match possible in the XRD peaks. Another parameter that is important to mention are a and b parameters on the unit cell. These parameters were adjusted to give always the exact minimum space needed

for the atoms to be contained. Most of this process was on a trial and error base, each time a crystal produced a similar XRD pattern when compared with the sample new variations of that crystal were made until the best possible match was found.

The matching process using the XRD was done on a selected area where there was a high probability of finding peaks corresponding to a ternary phase. This area was designated from the 2θ angles of 20^{o}-55^{o}. The peaks that fall between the AlB_2 and MgB_2 and had no other match were targeted for the purpose of creating a match with the crystallographic software.

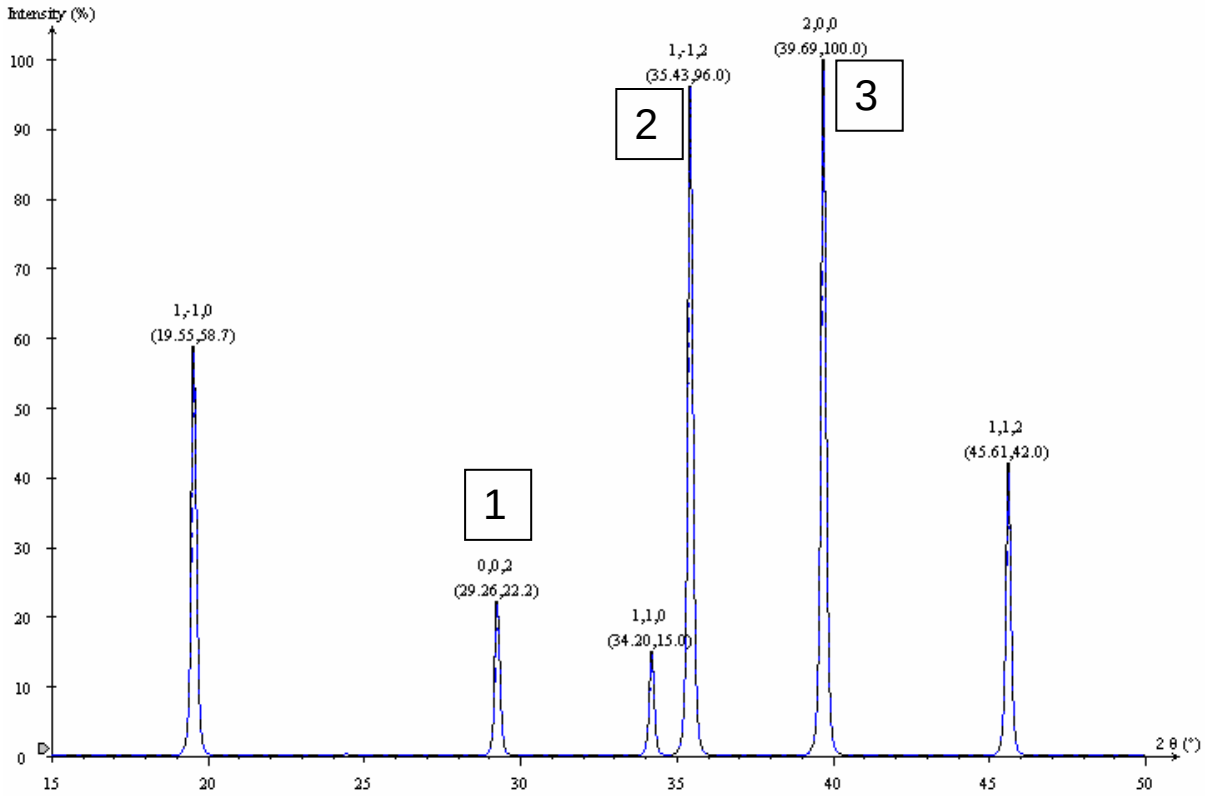

Figure 4.21 CARIne XRD pattern bearing the ternary phase of the composites samples

The final results produced a match on four of the studied peaks (figure 4.17, 4.21). These are found on the 2θ angles 29.2^{o}, 35.43^{o} and 39.69^{o}. This last angle, 39.52^{o} corresponds to the highest intensity peak for the modeled crystal.

This indicates a positive match between the sample and the model. The parameters for this crystal cell are a=5.24Å, b=5.24 Å, c=6.1 Å, α=90o, β=90o and γ=120o. The stoichiometric composition of this phase can now be calculated by counting the number of atoms found on a unit cell. The resulting composition is $Al_{0.5}Mg_{0.5}B_2$. This result can be explained with the fact that aluminum and magnesium have almost the same electronegativities and atomic radii, which make them easily, substitute each other. For a normal cell containing AlB_2, or MgB_2 there are half the number of aluminum and magnesium on the $Al_{0.5}Mg_{0.5}B_2$ crystal.

4.3.2 Crystallographic Model

The following drawings represent the model of a proposed crystallographic structure for the ternary diboride with a final stoichiometric composition of $(Al_{0.5}Mg_{0.5})B_2$. Figure 4.22 is a 3D-View of Crystallographic model designed with CARIne v3.1 software.

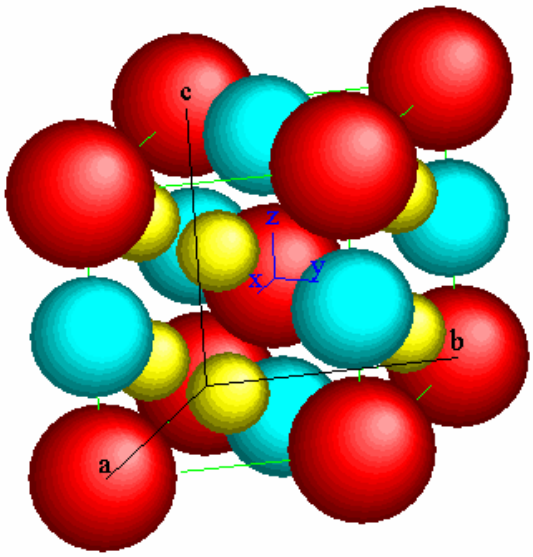

Figure 4.22 A 3D-view crystallographic model $(Al_{0.5}Mg_{0.5})B_2$ composite

The crystal is composed by three atomic layers (planes): the first layer has one atom of magnesium (color blue) and one atom of aluminum (red color) on the center of the plane (112). The second layer is composed of atoms of aluminum at (0 0 $\frac{1}{2}$) with one atom of magnesium on its center ($\frac{1}{2}\frac{1}{2}\frac{1}{2}$). The last plane repeats the first one. Between each layer there are 4 atoms of boron (yellow color). Figures 4.23 and 4.24 show a top and a front views of the crystal designed.

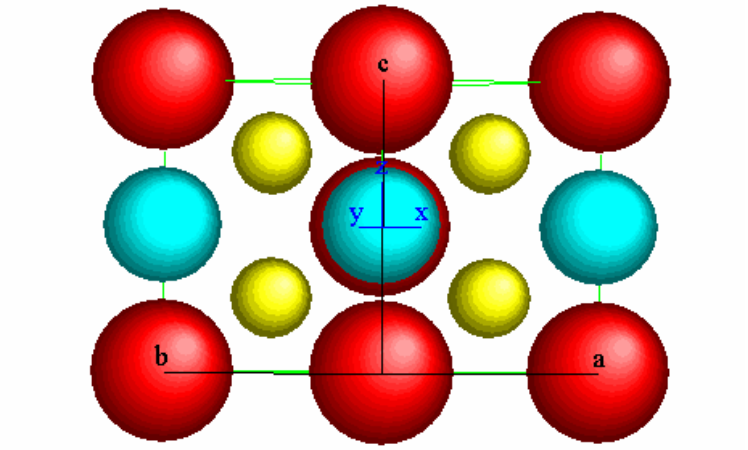

Figure 4.23 Top view crystallographic model $(Al_{0.5}Mg_{0.5})B_2$ composite

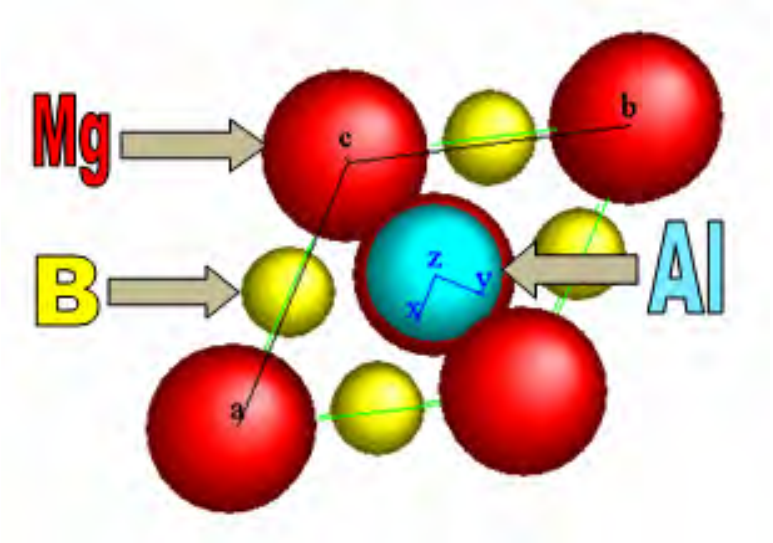

Figure 4.24 Front view crystallographic model $(Al_{0.5}Mg_{0.5})B_2$ composite

5 DISCUSSION

The aluminum atoms reacted with the magnesium diboride forming $(AlMg)B_2$. Al atoms substitute Mg atoms in the MgB_2 crystal as appreciated in the micrographs. Furthermore MgB_2 is not thermodynamically stable in contact with liquid Al since is forming a ternary phase, a solid solution with the matrix and the eutectic phase. The ballmilling process promoted two different ranges of reinforcement particles, the micrometric and nanometric dispersoids.

$(AlMg)B_2$ particles increased the hardness of the aluminum matrix. The hardness increases with the increment of reinforcement volume fraction and decreases with increment in particle size. The hardness of the reinforcements could not be determined. There was higher amount of nanodispersed particles for Al-5wt%MgB_2 composites and the HV matrix of this composite was also higher than samples containing 10wt%MgB_2.

EDS analysis confirmed $(AlMg)B_2$ ternary phase achieved after the selected process of synthesis. The evidence of $(AlMg)B_2$ nanoparticles was determined via SEM analysis.

XRD showed peaks between AlB_2, Al, MgB_2 from 20° to 45° associated with the $(AlMg)B_2$ ternary phase. CARIne crystallographic software, helped determine the probable stoichiometric composition of the ternary compound $(Al_{0.5}Mg_{0.5})B_2$ based on the XRD patterns of the composite samples.

DTA revealed the presence of a reaction probably associated with the ternary phase found. More extensive analysis with this technique should the implemented.

6 CONCLUSIONS

1. A technique of encapsulation in quartz tubes was developed to process the samples under vacuum for the melting reaction

2. The proposed extension in the Al-Mg-B ternary phase diagram up to 100% helped to trace the selected composition in this research

3. The ballmilling process with the selected parameters was the key process to achieve intimate contact between Al and MgB_2 via mechanical alloying

4. The demonstrated high hardness and low density of $(AlMg)B_2$-based composites make this processing route an alternative to high-strength and lightweight materials

5. Crystallographic sofware CARIne assisted on the determination of a crystal structure and its approximated stoichiometric composition

7 RECOMMENDATIONS

The ternary system aluminum-magnesium-boron has not wide information available. The author of this research recommends continuing with the project in the following fields:

1. To increase the number of nanoparticles in to the composite alloy, the increasing in the BPR parameter plays an important role for this goal, as well as application of temperature in the vial. Furthermore the increasing in the BPR will lead to higher values of hardness in the whole composite. BPR can be increased also using WC balls and higher balls diameter (20-25 mm). In addition pre-ballmilling the MgB_2 powder should also promote more nanoparticles on the aluminum matrix.

2. The use of process control agents (PCA) [6],[21] to reduce cold welding in the grinding medium, and the employment of Al nanosized, are examples that can be implemented to increase the milling time and therefore the nanometer-sized particles in the composite.

3. Using techniques such as TEM could confirm the extent of amorphization in the milled reinforcement.

4. Perform nanoidentation test to confirm the hardness of the $(AlMg)B_2$ composite and nanocomposites

5. More extensive DTA analysis of the composite

6. Perform mechanical testings of the composite to determine its strength

7. Characterize the electrical conductivity of the samples

8 REFERENCES

[1] Chawla, K. Composite materials: science and engineering. Springer-Verlag. New York; 1987. p.22

[2] Harris B. Engineering composite materials. Second Edition; IOM communications editors. 1999, p.20-7.

[3] Economy J, Deppisch C. Aluminum/Aluminum Diboride Metal Matrix Composites and Effect of Cooling Rate on the Crystallization of AlB_2 Flakes. SAMPE 18; 1973, p. 340-368.

[4] Suarez O. M. Mechanical properties of novel aluminum matrix composite containing boron. Journal of the mechanical behavior of materials. 2001; Vol 12, No. 4. p.226.

[5] Materials science international team, MSIT®. Light metals, part 1group 4 Ternary alloy systems, phase diagrams, crystallographic and thermodynamics data. Subv.A. Landolt-Bornstein. 2004, Vol 11. p.3.

[6] Hall A, Economy J. The $Al_{(L)} + AlB_{12} \leftrightarrow AlB_2$ Peritectic Transformation and Its Role in the Formation of High Aspect Ratio AlB_2 Flakes. Journal of Phase Equilibria. ASM International; Vol. 21; 2000, p.63-69.

[7] Bussman A., Bianconi A. The Tc amplification by quantum interference effects in diborides. Max-Planmck Insitute.Germany. 2003, p.2-4.

[8] Suryanarayana C. Mechanical Alloying and Milling. Marcel Dekker, New York; 2004, p.15-30

[9] Dunlap R, Small D, MacKay G. Materials preparation by ball milling. Journal of physics; 2000; 78: p.211-229.

[10] www.acgroupinc.com

[11] Bud'ko A., Lapertot G. Boron isotope effect in superconducting MgB_2. Physical review letters. 2001; Vol. 86, No.9.

[12]http://www.ifw-dresden.de/publications/annual-reports-1/annualreport-2001/13_16_2001.pdf

[13] Duschanek H, Rogl P. The Al-B system. Journal of Phase Equilibria. 1994. Vol 15; No. 5. p.10-11.

[14] Loa I, Kunc K, Syassen K. Crystal structure and lattice dynamics of AlB_2 under pressure and implications for MgB_2. Condensed matters 2002;29:15-24.

[15] Xu Z, Picu R. Dislocation-solute cluster interaction in Al-Mg binary alloys. Institute of physics publishing 2006, Vol.14; No.3. p.4-5

[16] http://www.ae.utexas.edu/courses/ase324_huang/Lecture6.pdf

[17] Totten G, Scott. Handbook of aluminum. Physical Metallurgy and Processes. Marcel Denkker;.New York 2003. Vol 1. p.77

[18] Totten G, D Scott. Handbook of Aluminum. Alloy production and materials manufacturing. Marcel Denkker; N.Y.2003, Vol.2. p.67-8.

[19] R.Yosomiya. Adhesion and bonding in composites, N.Y. Marcell Dekker.1990. p.99-100

[20] Interfaces in composites. American society for testing and materials. STP 452, 1970. p.78-9

[21] Meyers M. Chawla K. Mechanical Metallurgy, principles and applications. Prentice-Hall. 1984. p.41-4

[22] Shaw L, Zawrah W. Effects of Process-Control Agents on Mechanical Alloying of Nanostructured Aluminum Alloys. Metallurgical and materials transactions.2003. Vol. 34A. p.7

[23] http://www.indentec.com/Resources/Reference_Vickers_Test.pdf

[24] Software MATCH version 1.5b. Phase identification from powder diffraction. CRISTAL IMPACT

[25] Software CARIne Crystallography version 3.1

APPENDIX

APPENDIX A. Vario-Planetary Ball Milling Pulverisette 4 Fritsch™ software settings

1. Run setting for 8hr, 1000 rpm

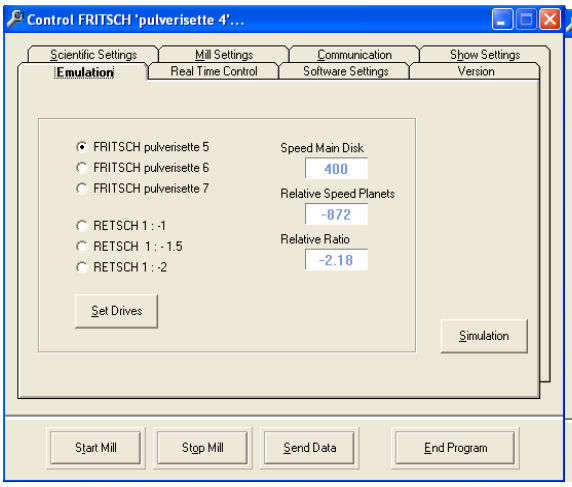

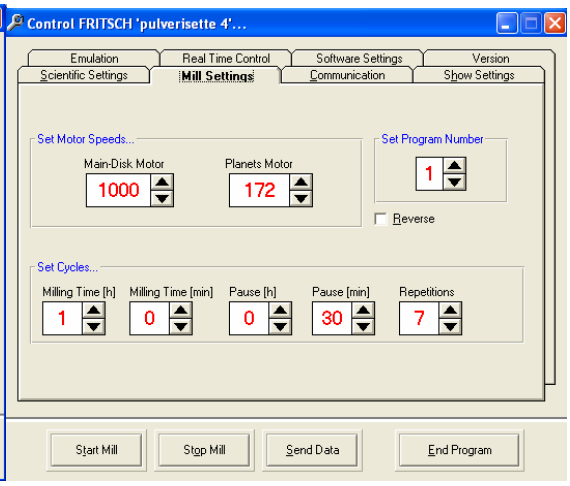

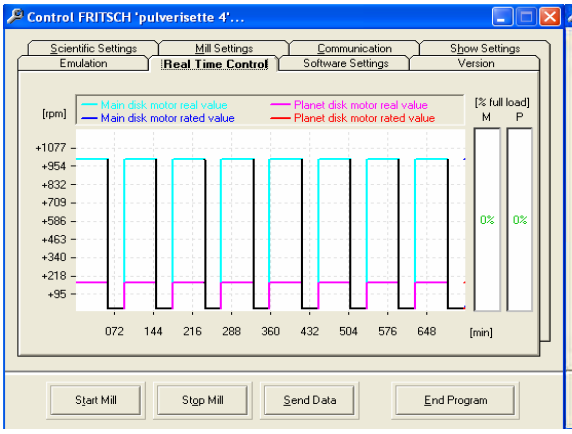

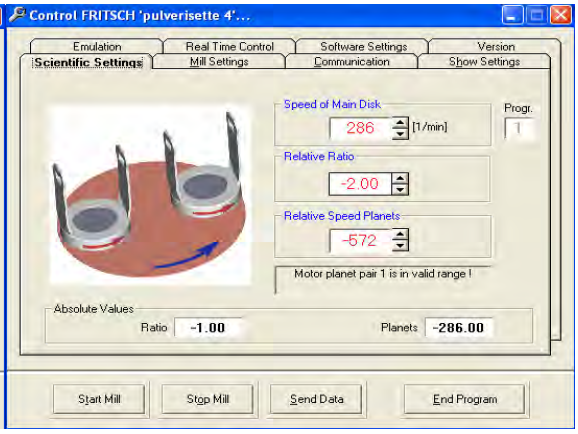

2. Run settings for 5hr, 600 rpm

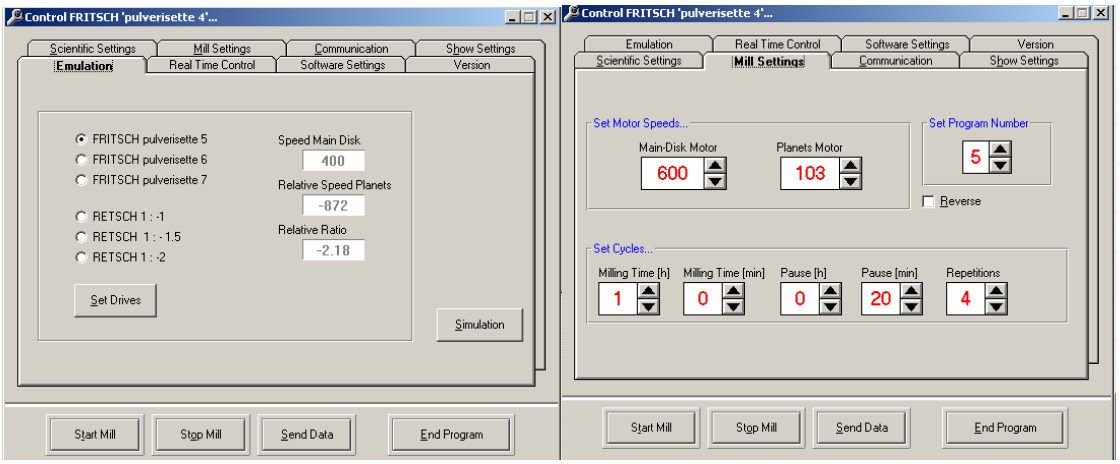

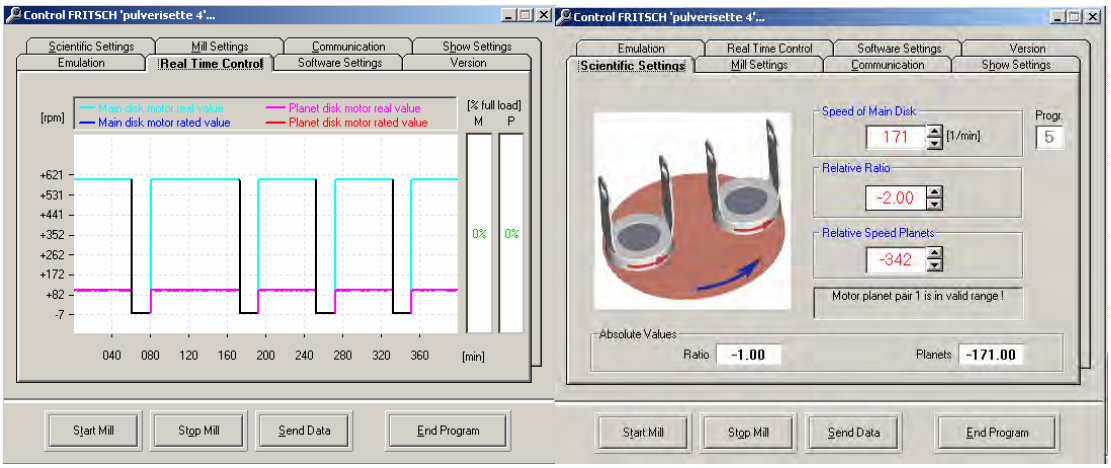

3. Run settings for 10hr, 800 rpm

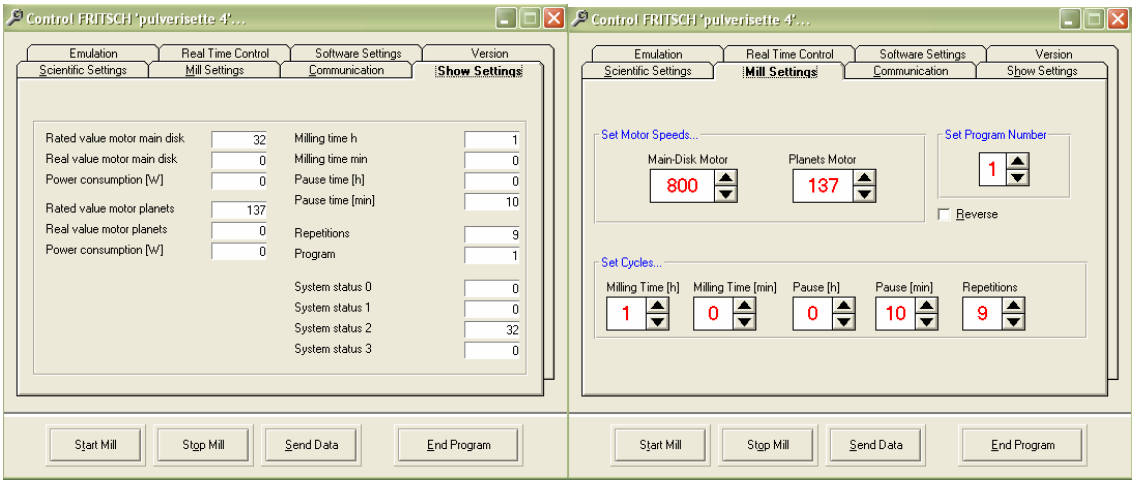

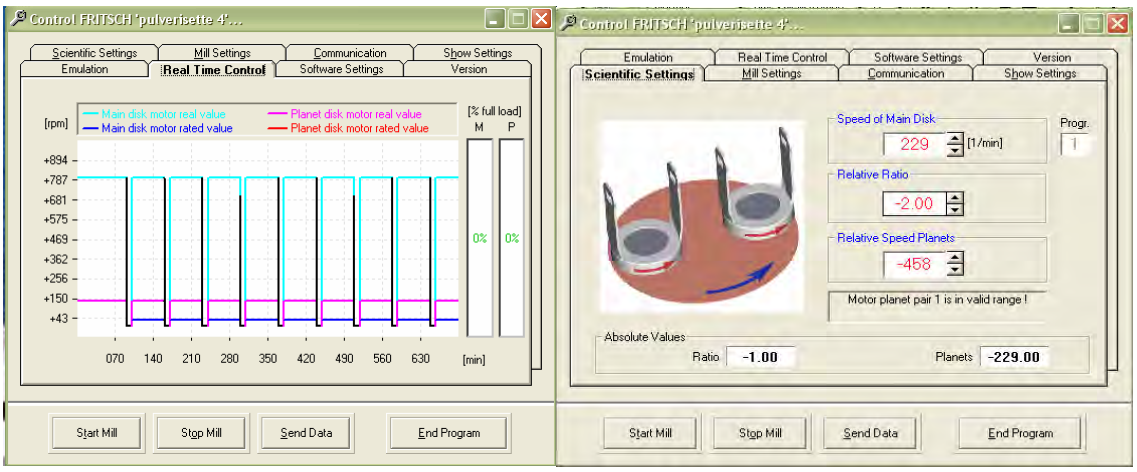

APPENDIX B. Examples of summary calculation using the IMAGE J program

1. Volume fraction or area fraction data in % for sample #1 at 500X

Summary of 500x,20 - Notepad

File Edit Format View Help

```
Threshold: 0-0
Count: 3638
Total Area: 261775.000 pixel^2
Average Size: 71.956 pixel^2
Area Fraction: 21.3%

Threshold: 0-0
Count: 2513
Total Area: 157687.000 pixel^2
Average Size: 62.749 pixel^2
Area Fraction: 12.8%

Threshold: 0-0
Count: 3187
Total Area: 284400.000 pixel^2
Average Size: 89.238 pixel^2
Area Fraction: 23.1%

Threshold: 0-0
Count: 3187
Total Area: 284400.000 pixel^2
Average Size: 89.238 pixel^2
Area Fraction: 23.1%

Threshold: 0-0
Count: 3770
Total Area: 233382.000 pixel^2
Average Size: 61.905 pixel^2
Area Fraction: 19.0%
```

2. Particle size data for sample #1 micrographs at 1000X

(Length column is the particle size in pixels)

Results175 - Notepad

File Edit Format View Help

	Label	Mean	Min	Max	BX	BY	Width	Height	Angle	Length
1	1000x,175		95.848	89.333	113.333	827	422	1	34	34
2	1000x,175		96.344	89.333	122.333	813	438	29	1	29
3	1000x,175		72.750	66.333	89	1077	251	6	34	34.525
4	1000x,175		72.803	67	81.667	1065	268	18	10	20.591
5	1000x,175		80.014	73.333	94.333	1117	546	16	17	23.345
6	1000x,175		74.698	65.333	84	1109	541	23	21	31.145
7	1000x,175		87.766	81	105	808	494	7	45	45.541
8	1000x,175		89.630	83	121.333	786	510	45	2	45.044
9	1000x,175		83.389	71	107.667	908	148	18	23	29.206
10	1000x,175		83.767	73.667	106.667	915	149	13	14	19.105
11	1000x,175		95.160	87.667	121.667	644	222	17	17	24.042
12	1000x,175		94.200	86.333	114.333	647	223	14	13	19.105
13	1000x,175		70.093	65.667	79	1208	472	14	10	17.205
14	1000x,175		75.944	68.667	87.333	1212	468	7	9	11.402
15	1000x,175		96.519	86.667	112	1038	577	5	6	7.810
16	1000x,175		112.417	108.667	114.333	1041	569	3	6	6.708
17	1000x,175		98.310	90.333	113.667	799	464	22	16	27.203
18	1000x,175		108.119	97.333	127.667	802	460	8	10	12.806

3. Set of windows displayed by Image J software while calculating volume fraction and particle size histogram (micrograph data for sample #7 at 200X)

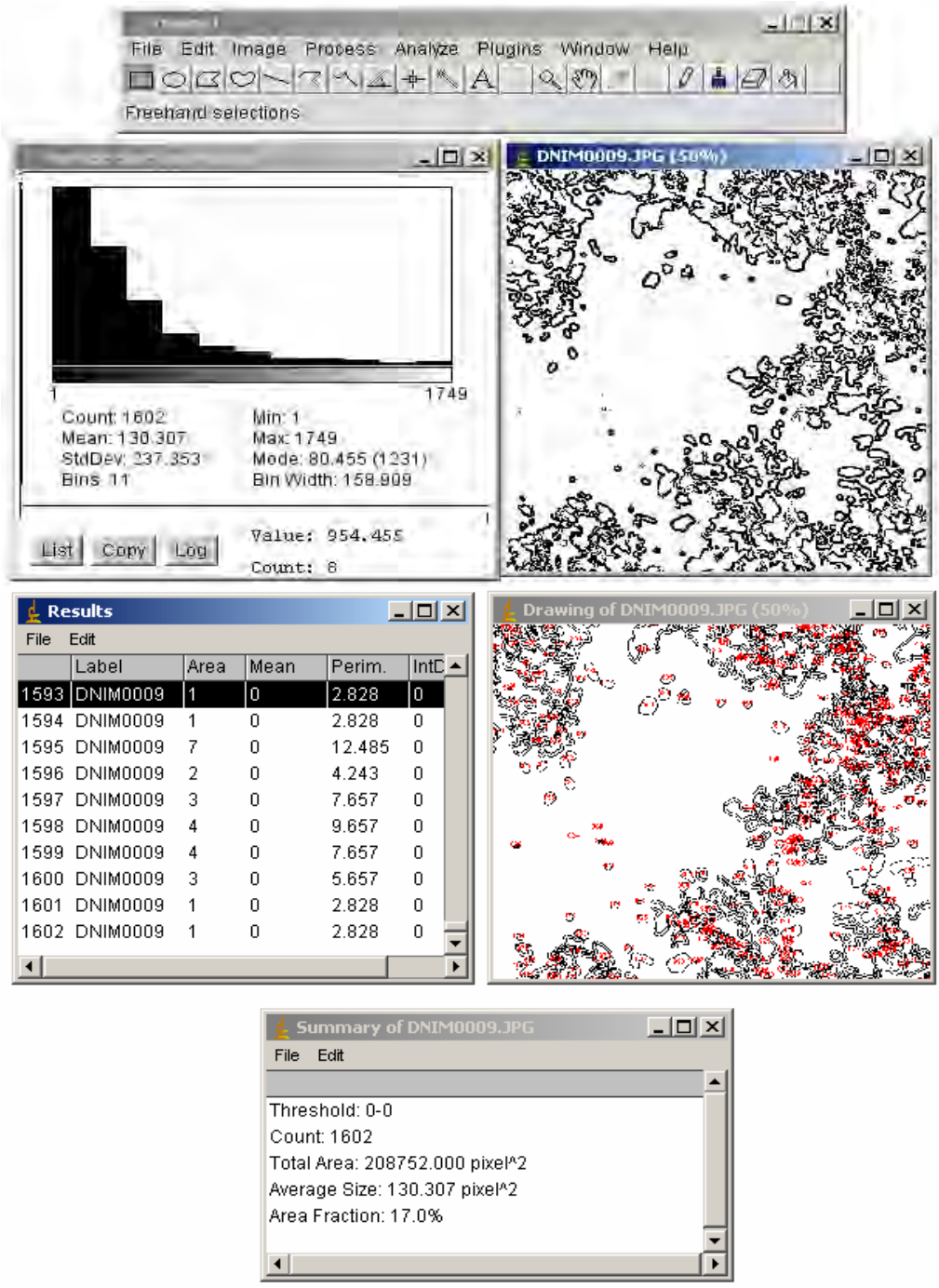

Appendix C. Display descriptive statistics of MINITAB 14 statistics software

1. Particle Size fig. 4.4, fig 4.5

Histogram and Interval Plot of 10%, 5%
Descriptive Statistics:
$10wt\%MgB_2$, $5wt\%MgB_2$

Variable	Total Count	N	N*	Mean	SE Mean	StDev	Variance	Minimum	Median
$10wt\%MgB_2$	414	414		3.610	0.159	3.236	10.470	0.237	2.562
$5wt\%MgB_2$	414	414		7.333	0.182	3.697	13.667	0.340	6.503

Variable	Maximum	Range
$10wt\%MgB_2$	20.230	19.993
$5wt\%MgB_2$	23.236	22.896

2. Volume Fraction, fig 4.6

Interval Plot of 10%, 5%
Descriptive Statistics: 10%, 5%

Variable	Total Count	Mean	StDev	Minimum	Median	Maximum
10%	57	23.73	8.88	11.90	22.40	47.80
5%	57	22.44	7.66	5.80	23.30	42.30

Probability Plot of $10wt\%MgB_2$, $5wt\%MgB_2$ fig. 4.8
Descriptive Statistics: $10wt\%MgB_2$, $5wt\%MgB_2$

Variable	Total Count	Mean	StDev	Minimum	Median	Maximum
$10wt\%MgB_2$	54	24.37	8.67	12.80	22.60	47.80
$5wt\%MgB_2$	54	23.209	7.102	8.000	23.800	42.300

3. Vickers microhardness, fig. 4.11

Welcome to Minitab, press F1 for help.
Retrieving project from file: 'C:\DOCUME~1\LUVINA\DESKTOP\DUREZA MATRIZ.MPJ'

Interval Plot of 10%, 5%
One-way ANOVA: 10%, 5%

Source	DF	SS	MS	F	P
Factor	1	3431.3	3431.3	40.03	0.000
Error	114	9771.1	85.7		
Total	115	13202.4			

S = 9.258 R-Sq = 25.99% R-Sq(adj) = 25.34%

Individual 95% CIs For Mean Based on Pooled StDev

Level	N	Mean	StDev	----+---------+---------+---------+-----
10%	58	32.655	7.059	(-----*-----)
5%	58	43.533	11.027	(-----*-----)

----+---------+---------+---------+----- 32.0 36.0 40.0 44.0

Pooled StDev = 9.258

Descriptive Statistics: 10%, 5%

Variable	Total Count	Mean	SE Mean	StDev	Minimum	Median	Maximum
10%	58	32.655	0.927	7.059	18.000	30.500	50.800
5%	58	43.53	1.45	11.03	23.70	45.30	74.20

4. Practical densities, fig. 18

Interval Plot
Descriptive Statistics: 10wt%, 5wt%

Variable	Mean	SE Mean	StDev	Minimum	Median	Maximum
10wt%	2.5472	0.0585	0.1940	2.2857	2.5400	2.9762
5wt%	2.5763	0.0286	0.0948	2.4423	2.5833	2.7174